

# The Hubble Space Telescope Key Project on the Extragalactic Distance Scale XXIV: The Calibration of Tully–Fisher Relations and the Value of the Hubble Constant

Shoko Sakai<sup>1</sup>, Jeremy R. Mould<sup>2</sup>, Shaun M.G. Hughes<sup>3</sup>, John P. Huchra<sup>4</sup>, Lucas M. Macri<sup>4</sup>, Robert C. Kennicutt, Jr.<sup>5</sup>, Brad K. Gibson<sup>6</sup>, Laura Ferrarese<sup>7,8</sup>, Wendy L. Freedman<sup>9</sup>, Mingsheng Han<sup>10</sup>, Holland C. Ford<sup>11</sup>, John A. Graham<sup>12</sup>, Garth D. Illingworth<sup>13</sup>, Daniel D. Kelson<sup>11</sup>, Barry F. Madore<sup>14</sup>, Kim Sebo<sup>2</sup>, N. A. Silberman<sup>14</sup>, and Peter B. Stetson<sup>15</sup>

*Draft version March 1, 2018*

## ABSTRACT

This paper presents the calibration of  $BVRIH_{0.5}$  Tully–Fisher relations based on Cepheid distances to 21 galaxies within 25 Mpc, and 23 clusters within 10,000 km s<sup>−1</sup>. These relations have been applied to several distant cluster surveys in order to derive a value for the Hubble constant,  $H_0$ , mainly concentrating on an I-band all-sky survey by Giovanelli and collaborators which consisted of total I magnitudes and 50% linewidth data for  $\sim 550$  galaxies in 16 clusters. For comparison, we also derive the values of  $H_0$  using surveys in B-band and V-band by Bothun and collaborators, and in H-band by Aaronson and collaborators. Careful comparisons with various other databases from literature suggest that the H-band data, whose magnitudes are isophotal magnitudes extrapolated from aperture magnitudes rather than total magnitudes, are subject to systematic uncertainties. Taking a weighted average of the estimates of Hubble constants from four surveys, we obtain  $H_0 = 71 \pm 4$  (random)  $\pm 7$  (systematic). We have also investigated how various systematic uncertainties affect the value of  $H_0$  such as the internal extinction correction method used, Tully–Fisher slopes and shapes, a possible metallicity dependence of the Cepheid period–luminosity relation and cluster population incompleteness bias.

## 1. INTRODUCTION

The Tully–Fisher relation, a luminosity–linewidth correlation for spiral galaxies, has become the most widely used method for determining galaxy distances independently of redshifts. Although the concept had been used variously, for example, by Öpik (1922) and Roberts (1969, 1975) over several decades, it was the groundbreaking paper by Tully & Fisher (1977: hereafter TF77) which laid out its potential as a powerful extra-galactic distance indicator. The Tully–Fisher (TF) relation is an empirical correlation between the absolute magnitude of a late-type spiral galaxy and its maximum rotational velocity. The latter quantity is usually determined from radio observations of the neutral hydrogen 21cm emission spectrum or from the optical rotation curve and is distance-independent. The TF relation has been used not only to investigate the density and velocity fields of the large-scale distributions of galaxies, but also to measure the value of the Hubble constant. Readers are referred to Dekel (1994), Strauss and Willick (1995) and Giovanelli (1997) for extensive reviews on these subjects.

After the first application of the TF relation using B-band photometry of spiral galaxies (TF77), it was soon discovered that there were mainly two advantages to using near-infrared

over visible–wavelength photometry: (1) the uncertainties due to interstellar absorption in both our own Galaxy and in the observed galaxy would be greatly reduced; and (2) the infrared emission is dominated by late-type giants and thus there is no significant dependence of mass-to-light ratio on galaxy morphology. The first study to apply the H-band (1.65  $\mu$ m) – HI linewidth TF relation was reported by Aaronson, Huchra & Mould (1980), who used a large-aperture H-band magnitudes to obtain distances to the M81, Sculptor and M101 groups. Aaronson and Mould (1983) later reported that in the infrared, the TF relation is morphology-independent, unlike in the blue where there is a small dependence. They also found that the slope in the relation is wavelength-dependent with its value increasing from the blue to IR. The scatter has been reported to be smaller for the infrared relation, making it a better distance indicator. Furthermore, the TF relation has been reported to be different for field and cluster galaxies or for galaxies in different clusters (Sandage and Tammann 1984).

Major improvement in the TF relation has been achieved during the late 1980s using CCD images. As a result, numerous all-sky surveys of spiral galaxies were carried out which used the TF relation to estimate their distances, to probe the density

<sup>1</sup>Kitt Peak National Observatory, National Optical Astronomy Observatories, Tucson AZ 85726, USA

<sup>2</sup>Research School of Astronomy & Astrophysics, Institute of Advanced Studies, Australian National University, Mount Stromlo Observatory Private Bag, Weston Creek, ACT 2611, Australia

<sup>3</sup>Institute of Astronomy, Cambridge, UK

<sup>4</sup>Harvard Smithsonian Center for Astrophysics, Cambridge, MA 02138, USA

<sup>5</sup>Steward Observatories, University of Arizona, Tucson AZ 85721, USA

<sup>6</sup>CASA, University of Colorado, Boulder, CO

<sup>7</sup>California Institute of Technology, Pasadena CA 91125, USA

<sup>8</sup>Hubble Fellow

<sup>9</sup>Carnegie Observatories, Pasadena CA 91101, USA

<sup>10</sup>Avanti Corp, 46871 Bayside Parkway, Fremont, CA 94538, USA

<sup>11</sup>Johns Hopkins University and Space Telescope Science Institute, Baltimore, MD 21218

<sup>12</sup>Department of Terrestrial Magnetism, Carnegie Institution of Washington, Washington, DC 20015, USA

<sup>13</sup>Lick Observatory, University of California, Santa Cruz CA 95064, USA

<sup>14</sup>IPAC, California Institute of Technology, Pasadena CA 91125, USA

<sup>15</sup>Dominion Astrophysical Observatory, Victoria, BC V8X 4M6, Canada

and velocity fields of the large-scale structure of the Universe. These include an r-band survey by Willick (1991) who used the 21cm linewidths to measure the rotation velocity, and also by Courteau (1992) who used the optical rotation curves. Han (1991) presented an I-band TF all-sky survey, which concentrated on the galaxies previously observed by Aaronson et al. (1982: hereafter AHM82) in their H-band survey. Most recently, Giovanelli et al. (1997: hereafter G97) presented an all-sky I-band survey of cluster galaxies out to  $\sim 10,000 \text{ km s}^{-1}$ . Mathewson et al. (1995) also measured I-band TF distances to clusters in the Southern hemisphere. Although the data have not been published as of now, Willick (1999) has presented a peculiar-velocity study based on his Las Campanas/Palomar Survey which is comprised of R-band photometry and  $H\alpha$  rotation curve observations of spiral galaxies out to  $10,000 \text{ km s}^{-1}$ . Dale et al. (1999) also has presented the velocity field study based on their I-band spiral-galaxy survey reaching as far out as  $\sim 25,000 \text{ km s}^{-1}$ . Courteau (1999) has also recently completed V and I-band photometric and  $H\alpha$  rotation-curve observations of spiral galaxies.

Although there is no firm physical basis for the TF relation, several groups have tried to recover the TF physical parameters using cosmological numerical simulations. Some examples include that by Steinmetz and Navarro (1999) who used high-resolution standard CDM simulations. They reported that the slope of the TF relation can be reproduced in a hierarchical clustering model naturally, suggesting that the TF relation is a direct consequence of the cosmological equivalence between the mass and circular velocity, which was also the conclusion of Mo, Mao & White (1998). On the other hand, Eisenstein & Loeb (1996) argued that because the scatter due to variations in formation histories is larger than that observed, the TF relation is a consequence of subsequent feedback processes which regulate the gas dynamics and star formation in these galaxies.

The main objective of the Hubble Space Telescope Key Project on the Extragalactic Distance Scale ( $H_0$  Key Project) is to measure the value of the Hubble constant to an accuracy of 10%. This is achieved by first obtaining precise Cepheid distances to nearby spiral galaxies and then by calibrating several secondary distance indicators. The  $H_0$  Key Project has now completed the observations of all of its target galaxies and the Cepheid data and distances for each galaxy have been presented as part of this series in papers I through XXIII. This paper presents research and analysis which are part of our final effort: the determination of the Hubble constant through the calibration of a variety of secondary distance indicators. In particular, this paper focuses on the calibration of the optical and near-IR TF relations using the Cepheid distances and the applications of the calibrated relations to distant cluster samples to determine the value of the Hubble constant. Other secondary distance indicators that are calibrated as part of the  $H_0$  Key Project are the surface brightness fluctuation method (Ferrarese et al. 2000a), Type Ia supernovae (Gibson et al. 2000) and fundamental plane (Kelson et al. 2000). The measurements of the Hubble constant will then be combined together in a consistent fashion in Mould et al. (2000). The extrapolation from a local value of the Hubble constant to the global value will be discussed in Freedman et al. (2000).

We have obtained new BVRI surface photometry of most of the galaxies suitable for the absolute calibration of the TF relation. These data are presented in Macri et al. (2000) and summarized in Section 2. The photometric data will be combined with the rotational velocity data compiled from the literature to

calibrate TF relations in these four optical wavelengths and in H band (Section 3). We also address the values of the intrinsic dispersion of the TF relations and the role played by a second parameter and non-linearities. The calibrated TF relations are then applied to distant clusters, mainly those from the I-band survey presented by Giovanelli et al. (1997a). The I-band TF distances to those clusters and values of  $H_0$  are presented in Section 4. They are then compared with values obtained by examining surveys at other wavelengths. In Section 5, various systematics that could affect the measurement of the  $H_0$  are examined. These include: (1) consistency between the calibrators and cluster samples; (2) dependence on the TF slopes and shapes; (3) dependence on the internal extinction correction method used; (4) metallicity dependence of the Cepheid period-luminosity relations; (5) large-scale velocity field of the Universe; and (6) cluster population incompleteness bias. Finally in Section 6, our  $H_0$  values are compared with previously derived TF  $H_0$  estimates.

## 2. DATA

### 2.1. Cepheid Distances

In Table 1, we list the spiral galaxies used in the TF analysis and the sources of their Cepheid distances. The list is comprised of: (1) 15 galaxies which were observed as part of the  $H_0$  Key Project, (2) 3 galaxies whose Cepheid distances were measured by other groups using the HST, and (3) 3 galaxies with Cepheid distances determined from ground-based observations. Note that there are several galaxies, such as NGC 4321 (M100) and NGC 5457 (M101), that have been observed by the Key Project but are not suitable for calibrating the TF relation because their inclinations are too small.

The distances given in Table 1 were all taken directly from the references as indicated. However, the corresponding errors were re-estimated so that they are consistent from galaxy to galaxy, as the understanding of uncertainties in Key Project Cepheid distances have grown over the course of the project. The details of which and how uncertainties were treated are found in Ferrarese et al. (2000b).

### 2.2. Photometry of Tully–Fisher Calibrators

We summarize briefly in this section the surface photometry observations and results, as this subject is presented in full detail by Macri et al. (2000). BVRI observations of the Tully–Fisher calibrator galaxies were conducted between March 1994 and May 1999 using the Fred L. Whipple Observatory 1.2-m telescope and the Mount Stromlo and Siding Springs Observatories 1-m telescope. Exponential disks were fitted to the surface brightness profiles, following Han (1992), to extrapolate total magnitudes. Both the profile fitting and the determination of the inclination were done interactively, in a manner similar to Giovanelli et al. (1997a).

For the IR data, we use  $H_{0.5}$  magnitudes presented by Aaronson et al. (1982), since with the exception of some work by Bernstein et al. (1994), that is all that is currently available in the literature, in terms of a consistent set of magnitudes between the calibrators and cluster galaxies.

#### 2.2.1. Corrections Applied to the Photometric Data

For the TF application, the photometric data were then corrected for Galactic extinction ( $A_{G,\lambda}$ ), internal extinction ( $A_{int,\lambda}$ ) and k-correction. The Galactic extinction values were estimated using the  $100\mu\text{m}$  maps reprocessed from IRAS/ISSA and

TABLE 1  
Cepheid Distances

Galaxy	Type	$m - M$ (mag)	Reference	Project
NGC 224	3	$24.44 \pm 0.10$	Freedman 1990	ground-based
NGC 598	6	$24.64 \pm 0.09$	Freedman 1990	ground-based
NGC 925	7	$29.84 \pm 0.08$	Silbermann et al. 1996	H <sub>0</sub> KP
NGC 1365	3	$31.39 \pm 0.20$	Silbermann et al. 1999 / Ferrarese et al. 2000	H <sub>0</sub> KP
NGC 1425	3	$31.81 \pm 0.06$	Mould et al. 1999 / Ferrarese et al. 2000	H <sub>0</sub> KP
NGC 2090	5	$30.45 \pm 0.08$	Phelps et al. 1998	H <sub>0</sub> KP
NGC 2403	6	$27.51 \pm 0.24$	Madore & Freedman 1991	ground-based
NGC 2541	6	$30.47 \pm 0.08$	Ferrarese et al. 1998	H <sub>0</sub> KP
NGC 3031	2	$27.80 \pm 0.08$	Freedman et al. 1994	H <sub>0</sub> KP
NGC 3198	5	$30.80 \pm 0.06$	Kelson et al. 1999	H <sub>0</sub> KP
NGC 3319	3	$30.78 \pm 0.12$	Sakai et al. 1999	H <sub>0</sub> KP
NGC 3351	3	$30.01 \pm 0.08$	Graham et al. 1997	H <sub>0</sub> KP
NGC 3368	2	$30.20 \pm 0.10$	Tanvir et al. 1995/Gibson et al. 2000	HST
NGC 3621	7	$29.13 \pm 0.11$	Rawson et al. 1997	H <sub>0</sub> KP
NGC 3627	3	$30.06 \pm 0.17$	Saha et al. 1999/Gibson et al. 2000	HST
NGC 4414	5	$31.41 \pm 0.10$	Turner et al. 1998	H <sub>0</sub> KP
NGC 4535	5	$31.10 \pm 0.07$	Macri et al. 1999 / Ferrarese et al. 2000	H <sub>0</sub> KP
NGC 4536	4	$30.95 \pm 0.08$	Saha et al. 1996/Gibson et al. 2000	HST
NGC 4548	3	$31.04 \pm 0.23$	Graham et al. 1999	H <sub>0</sub> KP
NGC 4725	2	$30.57 \pm 0.08$	Gibson et al. 2000 / Ferrarese et al. 2000	H <sub>0</sub> KP
NGC 7331	3	$30.89 \pm 0.10$	Hughes et al. 1998	H <sub>0</sub> KP

COBE/DIRBE data by Schlegel et al. (1998). The  $I$ -band cosmological  $k$ -term was adopted from Han (1992):  $k_I = 0.16z$ .

The amount of internal extinction in spiral galaxies and its correction methods still remains a very controversial issue. Several papers on this issue include Holmberg (1958), Valentijn (1990), Han (1992), Giovanelli et al. (1994), Burstein, Willick & Courteau (1994), Tully et al. (1998). For the internal extinction corrections, we have decided to apply those derived by Tully et al. (1998: hereafter T98), which are functions of both major-to-minor axes ratio ( $a/b$ ) and linewidth, and are expressed as:

$$A_{int,BRIK}^{T98} = \gamma_\lambda \log(a/b), \quad (1)$$

where  $\gamma_\lambda$  is a function of linewidth:

$$\gamma = \begin{cases} (1.57 + 2.75(\log(W_{20\%}) - 2.5)) & \text{B} \\ (1.15 + 1.88(\log(W_{20\%}) - 2.5)) & \text{R} \\ (0.92 + 1.63(\log(W_{20\%}) - 2.5)) & \text{I} \\ (0.22 + 0.40(\log(W_{20\%}) - 2.5)) & \text{K} \end{cases} \quad (2)$$

The idea behind the dependence on linewidth is that the light needs to travel further on average in a larger galaxy, thus requiring a larger extinction correction. However, it is noted that careful examination by Willick et al. (1996) revealed no dependence of the internal extinction on linewidth or luminosity.

In Appendix A, we review two other expressions for internal extinction derived by Han (1992) and Giovanelli et al. (1994). The main difference in these two studies is that the extinction corrections are dependent on the morphological types of galaxies. Mainly because the uncertainty in the morphological classification of distant galaxies is large, we have decided to use the T98 formulae in this paper. Later in Section 5.7, we will examine whether the value of  $H_0$  depends on the internal correction method.

The T98 corrections in Equation 1 include no independent formulae for the V and H bands. For these, we adopt the ratio  $A_V = 1.5A_I$  and  $A_H = 0.5A_I$ , which are reasonable values obtained by interpolating the T98 “extinction law” (Equations 1 and 2). Note that these ratios are slightly smaller than those derived by Cardelli, Clayton and Mathis (1989). This is to be

expected since Cardelli et al. used a fixed value for the optical path length, when in reality, blue light is attenuated more quickly than red, and thus different optical path lengths are sampled at different wavelengths (shorter in the blue than in the red) (Han 1992, T98).

Putting all the corrections together, the corrected apparent magnitude is then expressed as:

$$m_\lambda^c = m_{\text{obs},\lambda} - A_{G,\lambda} - A_{\text{int},\lambda} - k_\lambda \quad (3)$$

Note that the essential point for present purposes is to adopt *consistent* corrections between the calibrator and the distance galaxy samples. We emphasize that the corrections do not need to be optimum; they need to be consistent.

### 2.2.2. Inclination

Accurate measurement of inclination angles is crucial in the application of the TF relation since it is possibly the largest source of error in both magnitudes and linewidths. We measured the inclination in all four bands (BVRI), which agreed with each other well within  $1\sigma$  errors (see Macri et al. 2000 for details), which will be used in the rest of the paper to calibrate the TF relations and also to measure the value of  $H_0$ .

In Appendix B, we summarize the inclination information compiled from previously published data for each galaxy in detail. In some cases, such as NGC 1365 or NGC 4725, the kinematical inclination angle is quite different from the photometric inclination angles that we obtained. Although this could potentially lead to uncertainties in the corrected magnitudes and linewidths, this should not introduce a bias in our analysis: for the distant cluster surveys, which will be used to measure the value of the  $H_0$ , the inclinations of galaxies were measured strictly from the imaging, either on photographic plates or on CCDs. Because our main objective is to create a calibration sample that is consistent with the cluster surveys, only the photometric inclination angles (from Macri et al. 2000) will be considered for further analysis.

### 2.3. Linewidths

Although linewidths have been measured and published for all the Key Project galaxies selected as calibrators for the Tully–Fisher relation, we have endeavored wherever possible to re-measure the various linewidth definitions directly from the profiles, in order to check for any anomalies. We are grateful to Martha Haynes for allowing us access to the profiles of the KP galaxies which were observed as part of the Giovanelli et al (1997a) database. In addition, several 21cm line profiles were digitally scanned from the literature. We review here only briefly the linewidth database, as the details are explained in Macri et al. (2000).

In order to avoid systematic effects when applying our Cepheid calibration to various distant data sets, it is important that we use the applicable linewidth definition. The 20% linewidths,  $W_{20}$ , are often used in the TF applications, which are the width in  $\text{km s}^{-1}$  of the HI profile measured at 20% of the peak of the HI flux, where for a 2–horned profile this is taken as the mean of each horn’s peak flux. Another commonly used linewidth measurement is the 50% width, which is, for example, used in the I–band data set of G97. The  $W_{50}$  is the width at 50% of each of the horn maxima (or if the profile is Gaussian-shaped, then the width at 50% of the single peak). The potential advantage of measuring the linewidth at the 50% flux level is that it is less likely to be affected by noise, especially for low S/N profiles. However, the G97  $W_{50}$ ’s are measured from an interpolation between the levels at 15% and 85% of the peak flux. For unusual profiles, this can result in underestimated profile widths.

As all the KP galaxies are relatively nearby, most have very high S/N profiles. Many of them are also very large and overfill the telescope’s beamsizes. In these cases, to avoid systematically underestimating the profile widths, the observers have claimed to have been careful to ensure that a sufficient number of pointings were obtained.

Most galaxies have the classic steep-sided twin-horned profiles of normal edge-on spirals. Unfortunately, there are exceptions. Galaxies with different profiles are NGC 3031 (which is distorted by a tidal interaction with M82=NGC 3034), NGC 3319 (which has a low-level pedestal), and NGC 3368 (which has a non-symmetric two-horned profile). The  $W_{50}^G$  widths are particularly sensitive to both low S/N profiles and pedestal features (which affect the positions of the 15% level) and unusual profiles (as the 85% level can be far from the end of the steep edge), the latter leading to systematically underestimated widths. These cases are flagged by larger uncertainties.

### 2.3.1. Corrections Applied to the Linewidths

We apply the following corrections to the raw linewidth data. First, linewidths were corrected for the inclination angle ( $i$ ) and also for the redshift ( $z$ ) effect following:

$$W^c = W(\sin i)^{-1}(1+z)^{-1}. \quad (4)$$

The inclination angle is derived from the eccentricity measured on the CCD frames via:

$$i = \cos^{-1} \sqrt{\frac{(b/a)^2 - q_0^2}{1 - q_0^2}}, \quad (5)$$

where  $q_0$  is the intrinsic minor-to-major axis ratio of edge-on spiral galaxies for which we adopt  $q_0 = 0.13$  for  $T > 3$  and  $q_0 = 0.20$  for other types. No turbulence corrections are applied in this paper as the physical basis for this effect still remains ambiguous, except in estimating the internal extinction

corrections (in Section 3.2). Originally, one of the reasons for applying the turbulence correction was to straighten the TF relation, in addition to some theoretical preconceptions. Furthermore, as we will discuss in later sections, the calibration galaxies for our multi-wavelength TF relations mostly populate the region where the linewidths exceed  $\sim 300 \text{ km s}^{-1}$ . Since the turbulence correction is very small and constant for luminous galaxies ( $\log W \geq 2.5$ ), applying a turbulence correction would have no significant effect on our determination of  $H_0$ .

### 2.4. Data Presentation

In Table 2, we list all of the photometric, inclination and kinematical data used in calibrating the TF relation. The columns for Table 2 are: (1) name of the galaxy; (2)–(6)  $BVRI$  total and  $H_{0.5}$  aperture magnitudes corrected for Galactic extinction and internal extinction, as described in Section 2.2. For raw, uncorrected magnitudes, see Macri et al. (2000). The photometric data for NGC 224, NGC 598, NGC 2403 and NGC 3031 were taken directly from Pierce and Tully (1992); (7) logarithmic 20% linewidth corrected for inclination (using the mean inclination) and redshift; (8) logarithmic 50% linewidth corrected for inclination and redshift; (9) photometric I–band inclination; and (10) the mean photometric inclination which is used to calculate the internal extinction, and also to correct for inclination for the linewidths. We list here the I–band photometric inclination angles, since the strategy is to bring our photometry/linewidth data to the same system as the distant cluster surveys. As will be described in detail later on, the I–band survey by G97 estimated the galaxy inclinations from their I–band images. We note, however, that in most cases, the  $BVRI$  photometric inclinations agree with each other extremely well, within  $1\sigma$  errors.

## 3. CALIBRATION OF MULTI-WAVELENGTH TULLY–FISHER RELATIONS

In this section, we derive TF calibrations using two independent methods. The first is to obtain a consistent set of  $BVRIH_{0.5}$  TF relations such that we can compare and examine the dispersions and the role of second parameters. This is done by using only the calibrator galaxies with directly-measured Cepheid distances. The 20% linewidths and the mean photometric inclination angles estimated from  $BVRI$  measurements will be used in this case. The second method is to derive TF calibrations that can actually be applied to the distant cluster surveys to estimate  $H_0$ . This is done by using appropriate linewidth and inclination angles, and also incorporating the cluster galaxy data to calculate the TF slopes.

### 3.1. TF Calibration using Nearby Calibrator Galaxies Only

First, we present  $BVRIH_{0.5}$  TF relations for 20% linewidth, using the mean of the  $BVRI$  photometric inclination angles (Col 10 of Table 2), derived from 21 nearby galaxies with Cepheid distances only. While the optical photometric data,  $BVRI$ , are all total magnitudes, the H–band magnitude,  $H_{0.5}$  is an aperture magnitude, extrapolated to the radius equivalent to half the total blue light of the galaxies. Slopes and zero points are determined using bivariate linear fits, minimizing errors in both  $\log W^c$  and  $M^c$ :

$$B_T^c = -7.85(\pm 0.71)(\log W_{20}^c - 2.5) - 19.70(\pm 0.11) \quad (6)$$

TABLE 2  
Photometric and Kinematical Data for Tully–Fisher Calibrators

Galaxy	$B_T^c$ <sup>a</sup> mag	$V_T^c$ <sup>a</sup> mag	$R_T^c$ <sup>a</sup> mag	$I_T^c$ <sup>a</sup> mag	$H_{-0.5}^c$ <sup>a</sup> mag	$\log W_{20}^c$ <sup>b</sup> kms <sup>-1</sup>	$\log W_{50}^c$ <sup>b</sup> kms <sup>-1</sup>	$i_T^c$ deg	$\tilde{r}^c$ deg
N224 <sup>d</sup>	-21.37 (19)	...	-22.47 (18)	-23.04 (18)	-23.83 (11)	2.744(28)	2.703(30)	78(2)	78(2)
N598 <sup>d</sup>	-18.57 (18)	...	-19.39 (18)	-19.80 (18)	-20.31 (11)	2.397(74)	2.357(82)	54(2)	54(2)
N925	-19.59 (29)	-19.95 (16)	-20.24 (16)	-20.59 (28)	-21.16 (10)	2.420(49)	2.384(52)	56(1)	56(2)
N1365	-21.86 (37)	-22.30 (12)	-22.71 (17)	-23.38 (12)	-24.30 (11)	2.682(35)	2.626(32)	62(3)	55(2)
N1425	-20.96 (17)	-21.42 (08)	-21.82 (07)	-22.38 (08)	-23.07 (08)	2.621(41)	2.599(43)	64(1)	63(1)
N2090	-19.83 (11)	-20.20 (10)	-20.67 (10)	-21.26 (11)	-21.95 (10)	2.501(35)	2.493(38)	64(1)	67(2)
N2403 <sup>d</sup>	-19.11 (29)	...	-19.93 (28)	-20.32 (28)	-21.14 (25)	2.480(59)	2.457(62)	58(2)	58(2)
N2541	-18.72 (18)	-19.09 (13)	-19.37 (10)	-19.82 (13)	-20.24 (10)	2.370(49)	2.361(52)	58(2)	62(1)
N3031 <sup>d</sup>	-20.64 (17)	...	-21.87 (17)	-22.43 (17)	-23.54 (10)	2.719(34)	2.654(39)	58(2)	58(2)
N3198	-20.28 (08)	-20.75 (08)	-21.07 (07)	-21.55 (08)	-22.22 (08)	2.531(32)	2.506(34)	71(2)	68(2)
N3319	-19.34 (14)	-19.69 (14)	-19.94 (13)	-20.32 (14)	-20.44 (13)	2.405(48)	2.364(51)	60(1)	58(1)
N3351	-19.78 (11)	-20.56 (09)	-21.00 (09)	-21.61 (09)	-22.56 (10)	2.586(47)	2.577(42)	45(2)	45(2)
N3368	-20.47 (14)	-21.26 (12)	-21.73 (11)	-22.29 (11)	-23.41 (11)	2.674(36)	2.631(34)	51(1)	49(1)
N3621	-19.48 (12)	-20.00 (12)	-20.50 (12)	-20.99 (12)	-21.84 (12)	2.499(35)	2.471(38)	64(1)	66(1)
N3627	-21.10 (18)	-21.73 (18)	-22.12 (18)	-22.63 (18)	-23.50 (18)	2.626(26)	2.694(35)	65(1)	65(1)
N4414	-20.88 (13)	-21.57 (11)	-21.98 (11)	-22.59 (11)	-23.65 (11)	2.743(39)	2.562(39)	46(2)	46(2)
N4535	-20.80 (10)	-21.38 (09)	-21.61 (08)	-22.27 (08)	-22.72 (09)	2.586(38)	2.538(32)	49(1)	51(1)
N4536	-20.49 (12)	-21.05 (10)	-21.39 (09)	-21.95 (13)	-22.79 (09)	2.562(30)	2.695(31)	68(1)	69(1)
N4548	-20.36 (24)	-21.04 (23)	-21.47 (23)	-22.13 (23)	...	2.617(46)	2.729(25)	38(1)	39(1)
N4725	-21.27 (10)	-21.85 (09)	-22.20 (09)	-22.74 (09)	-23.65 (10)	2.671(26)	2.564(30)	51(1)	62(1)
N7331	-21.58 (12)	-22.30 (11)	-22.73 (11)	-23.29 (11)	-24.66 (11)	2.746(21)	2.576(45)	68(2)	69(2)

<sup>a</sup>The format of magnitudes is such that  $-21.65(13)$  is equivalent to  $-21.65 \pm 0.13$ .

<sup>b</sup>The format of  $\log W$  is such that  $2.682(35)$  is equivalent to  $2.682 \pm 0.035$ .

<sup>c</sup>The inclination errors are shown in brackets.

<sup>d</sup>Magnitudes from Pierce and Tully 1992

$$V_T^c = -8.81(\pm 0.82)(\log W_{20}^c - 2.5) - 20.27(\pm 0.12) \quad (7)$$

$$R_T^c = -8.68(\pm 0.71)(\log W_{20}^c - 2.5) - 20.60(\pm 0.11) \quad (8)$$

$$I_T^c = -9.21(\pm 0.75)(\log W_{20}^c - 2.5) - 21.09(\pm 0.12) \quad (9)$$

$$H_{-0.5}^c = -11.03(\pm 0.86)(\log W_{20}^c - 2.5) - 21.74(\pm 0.14) \quad (10)$$

In Figure 1, the above TF relations are plotted. The *observed* dispersions of above relations are  $\sigma = 0.45, 0.37, 0.35, 0.37$  and  $0.36$  for BVRI and  $H_{-0.5}$  respectively, which are combinations of observational errors and intrinsic scatter of the Tully–Fisher relations themselves. The latter will be discussed in Section 3.4. Errors in  $\log W$  and absolute magnitudes were determined as follows. The linewidth error is a combination of two sources: the observational error in the linewidth measurement and the uncertainty in the inclination angle. For absolute magnitudes, their uncertainties come from a few sources including the uncertainty in the Cepheid distance modulus (random only, typically  $\sim 0.10$  mag), observational photometric error (typically  $\sim 0.10$  mag), the error in internal extinction law which is associated with the error in the inclination angle, and the uncertainty in the Galactic extinction ( $\sim 0.02$  mag in I-band).

We have also calculated the slope and zero point of each TF relation using the direct and inverse fits for each wavelength as a consistency check, in which the fits were determined by minimizing the errors in magnitudes and linewidth only respectively. Schechter (1980) suggested that the average value of  $\log W$  at a constant magnitude does not depend on whether the sample is distance- or magnitude-limited. That is, the inverse TF relation is insensitive to the incompleteness bias. Based on this, some authors have preferred to use the inverse TF relation to derive cluster distances (e.g. Tully 1999). Although the slopes do change slightly as expected depending on what fit is used, the zero point remains well within  $1\sigma$ . As will be shown

in Section 5.2.1, the TF slope uncertainty has a very little effect on the  $H_0$  value. In this paper, we will use the bivariate fits only. Several articles have investigated the possibility of a TF relation being a quadratic relation (cf: Mould, Han and Bothun 1989). We do not use quadratic TF relations in the main analyses of this paper, however, interested readers are referred to Appendix C for further discussion.

### 3.2. TF Calibration using Both the Calibrators and Cluster Galaxies

We can also calibrate TF relations by combining the local calibrator galaxies and cluster survey galaxies. These independent samples should supplement each others' advantages and disadvantages. The set of equations (6–10) will provide a consistent set of TF calibrations which can be used to investigate several fundamental questions pertaining to the TF correlation itself, which will be discussed in the following sections. However, in order to fulfill the original goal of this project, to measure the value of  $H_0$ , we must in addition derive TF equations that are exactly on the same photometric–linewidth system as the distant cluster surveys. Thus, a second set of the  $I$  TF relations was derived using slightly different methods.

The G97 I-band survey used I-band photometric inclinations. In determining the zero points and slopes, we take advantage of the all-sky survey data that are available. Calibrating the TF relations using only local galaxies with Cepheid distances poses two problems. This sample, which consists of only 21 galaxies, is not statistically large enough to constrain the slope very well, and errors in the individual galaxy distances contribute significantly to the final dispersion. To minimize the first problem, we iteratively determine the slope and zero point using both the distant cluster sample and the local calibrators as follows: (1) the slope and zero point are calculated using

the calibrator sample only. (2) Then distances to distant cluster galaxies (e.g. the G97 I-band sample) are determined using the calibration from (1), such that all the clusters are put on the same  $(\log W - 2.5) - M_I$  plane. Here, the cluster sample galaxies are corrected for the cluster incompleteness bias (which will be discussed in detail in Section 5.4). (3) The slope is determined using this combined cluster sample. (4) The zero point is then estimated by minimizing the dispersion in the local calibrating sample using the slope from (3). Steps (2) through (4) are repeated until the slope and zero point converge. Convergence is usually achieved within three or four iterations. We obtain the following I-band TF relation:

$$I_T^c = -10.00(\pm 0.08)(\log W_{50}^c - 2.5) - 21.32 \quad (11)$$

For reference, the I-band–50% TF relation derived using only the calibrators (equivalent to Equation 9) is:  $I_T^c = -9.87(\log W_{50}^c - 2.5) - 21.30$ , which is virtually the same as Equation 11. Finally, note that the internal extinction correction of T98 is expressed in terms of 20% linewidths. The G97 database, on the other hand, lists 50% linewidths. We have made a compilation of galaxies with both published 20% and 50% linewidths by examining the G97 survey and an H-band survey by Aaronson, Huchra, Mould and collaborators (cf. Aaronson et al. 1982). The mean ratio for 73 such galaxies is  $W_{20} = 1.1(\pm 0.03)W_{50}$ . When estimating the internal extinction, we calculate the corresponding 20% linewidth using this ratio for all the cluster galaxy data. In addition, the T98 internal extinction expressions are given as a function of turbulence-corrected linewidth. Thus, only in estimating the internal extinction, we apply this turbulence correction to the linewidths following Tully & Fouqué (1985).

### 3.3. Uncertainties in the Tully–Fisher Parameters

To better understand the errors in the derived TF relations, we generated a sample of 5000 random points which followed a Tully–Fisher relation of dispersion 0.43 mag. From this sample, 500 random subsamples of  $N$  galaxies were drawn, and the zero point and slope were calculated for each trial run. We examined three cases:  $N=25$ , 500 and 2000. For  $N=25$  trial runs, the range of slope distribution is  $\sim 5$  times larger than other two larger samples, suggesting that the sample solely consisting of the  $\sim 20$  Local calibrators could give a slope estimate that is significantly different from the true value. The cluster database used to estimate the TF slope was comprised of more than 500 galaxies (for the I-band survey). Even for this larger sample, the slope distribution has a  $1\sigma$  RMS scatter of 0.09 mag.

The distributions of zero points obtained for the same set of simulations were also examined. Again as expected, the smallest sample, in which 25 galaxies were picked during each trial run, has the largest standard deviation in the zero point distribution of 0.13 mag, which in fact agrees with the actual zero point error calculated in Equations 6–10.

We have determined the slope using a sample of  $\sim 500$  galaxies and then the zero point using a sample of  $\sim 20$  galaxies. Thus, we formally adopt the uncertainties for the slope and zero point of 0.09 and 0.13 mag respectively. In Section 5.5, the sensitivity of the value of  $H_0$  to the slope uncertainty of the TF calibration will be investigated further.

### 3.4. Dispersion

The dispersion of the TF relation has three primary origins: (1) intrinsic to the relation itself, due to departures from the

“perfect” physical correlations, such as Freeman’s exponential disk law, or variations in mass-to-light ratio, (2) observational errors in magnitude and linewidths, and (3) for the case of a cluster TF relation, the physical depth of the cluster itself or, for the case of the calibrators, the uncertainties in the distance estimates of the individual galaxies.

The subject of the TF dispersion has long been of interest, as its value can pose strong constraints on scenarios for galaxy formation and evolution. For example, Eisenstein and Loeb (1996) suggested that a dispersion exceeding 0.3 mag is expected for most galaxy formation histories. Silk (1996) speculated that a tight TF relation could suggest an unexpectedly late epoch of galaxy formation. It is also important to understand the intrinsic scatter of the TF relation, because it is directly related to the bias in the distance ladder itself.

Surprisingly, estimates of dispersion have been very ambiguous, ranging from  $\sim 0.1$  mag (e.g. Bernstein et al. 1994, Freedman 1990), up to  $\sim 0.7$  mag (e.g. Kraan–Korteweg et al. 1988, Sandage 1994, Tammann 1999), with many estimates around 0.2–0.3 mag (e.g. Pierce & Tully 1988, Willick 1991, Courteau 1992, Bothun & Mould 1987, Schommer et al. 1993). More recent studies have shown furthermore that the TF dispersion is a more complex function of galaxy types and sizes. Using his LCO/Palomar Survey, Willick (1999) found that the dispersion is as much as  $\sim 0.75$  mag for low-luminosity, low-surface brightness galaxies, while for the higher luminosity, higher surface brightness galaxies, it is  $\leq 0.35$  mag. Giovanelli (1997) reported that the dispersion of the TF relation is in fact a function of linewidth; it decreases from fast-rotators ( $\sigma \sim 0.2$  mag for  $\log W \sim 2.6$ ) to slow-rotators ( $\geq 0.3$  mag for  $\log W < 2.2$ ). Readers are referred to Giovanelli (1997) and Willick (1999) for an extensive discussion on this subject. Here, we have a unique set of data: the local calibrator data provide a sample in which the distance to each galaxy is known with 10–15% accuracy unlike the case of the cluster TF relation, where the cluster depth can be an additional unknown parameter. Freedman (1990) also used galaxies with accurately measured Cepheid distances, but this sample now has 21 galaxies, instead of five used by Freedman (1990). Dispersions for BVRIH Tully–Fisher relations obtained from our Cepheid calibrator galaxies were quoted in Section 3.1. These are, however, observed dispersions and are a combination of observational errors and the intrinsic scatter of the TF relation itself, added in quadrature. We determined the intrinsic scatter of the TF relation for each wavelength, by estimating the observational error for each calibrator galaxy following Equation 10 of Giovanelli et al. (1997b). We have also assumed that the dispersion is a constant over the linewidth range  $2.4 \leq \log W \leq 2.8$  spanned by the calibrators. A typical observational error for galaxies is  $\sim 0.30 \pm 0.05$  mag, (whose main sources are photometric, distance modulus uncertainty and the linewidth measurement uncertainty multiplied by the TF relation slope,) indicating that the intrinsic dispersions are 0.25, 0.22, 0.25, 0.20 and 0.19 mag for B, V, R, I, and  $H_{0.5}$  respectively. We have tested to see if this dispersion is a function of some observational parameter, such as the color. In Figure 2, we plot TF residuals as a function of color, which show no dependence, suggesting that color is certainly not a candidate for the second parameter in TF relations.

Another question to be addressed is whether a dispersion of 0.20–0.25 mag is a value that could have been measured accidentally. In the previous section, the slope and zero point of the TF relation were examined using a randomly created sample of 5000 galaxies. A similar exercise is carried out here,

except a sample of 5000 points were generated assuming that the dispersion of the TF relation is 0.7 mag. A random subsample of galaxies was again withdrawn 500 times. The dispersion of 0.2 mag is highly unlikely, with a probability of practically zero. The B- and V-band TF relation dispersions were slightly higher than that of other wavelengths, measured at 0.25 mag. The chance of ‘accidentally’ observing even this dispersion is remote, less than 1%, if the true dispersion is 0.7 mag.

Furthermore, when the cluster data, consisting of few hundred galaxies, are put on the same TF plane, one finds that its dispersion is less than 0.3 mag. This confirms that the intrinsic dispersion of TF relation is relatively small.

### 3.5. Color Dependence of Tully–Fisher Relations

If the internal extinction correction were perfect, there should be no dependence of the corrected color of the TF galaxies on inclination. In Figure 3 (top), we examine the  $(B-I)$  color of the local calibrators as a function of inclination. The solid circles represent the data corrected using Equation 1, while the open circles indicate the uncorrected data. There is a slight dip in this color–inclination relation around the inclination angle of  $50^\circ$ , however, there is no overall trend that is observable. Also shown in the middle and bottom plots of Figure 3 are the  $(B-I)$  vs inclination relations for the same set of Local calibrator galaxies, but here, Han’s (Equation A1 in Appendix A) and Giovanelli et al.’s (Equations A2 and A3) extinction corrections, respectively, were used. Although for both Han’s and Giovanelli et al.’s corrections there may be a slight decline in the relation for the large–inclination region, this apparent trend could be partly due to small–number statistics. One significant question is whether the value of  $H_0$  is affected by the uncertainty arising from the internal extinction corrections. This will be discussed in detail in Section 5.7.

### 3.6. Barred Galaxies in the Tully–Fisher Relations

Among the 21 calibrator galaxies in our Tully–Fisher sample, seven are barred galaxies. In this section, we explore whether these barred galaxies are in fact suitable TF calibrators or not. On the left side of Figure 4, we have re-plotted B, I and H band TF relations using the 20% linewidth. Seven barred galaxies, NGC 925, NGC 1365, NGC 3319, NGC 3351, NGC 3627, NGC 4535, and NGC 4725 are shown with open circles. The solid line in each plot represents the TF fit to all the galaxies. A striking feature is that the majority of them lie above the TF relations, suggesting that they are systematically brighter for a given rotational velocity. This is true in all three wavelengths. (Although not shown here, the same applies to the V- and R-band TF relations). In Table B1, a summary of published photometric and kinematical inclination angles are listed. We use the kinematical inclination angles for the seven barred galaxies and plot the TF relation on the right side. The solid line in each plot shows the fit through all the galaxies, using the kinematical inclination angles for the barred galaxies. The dotted line is the fit through the TF relation using the photometric inclination angles for all galaxies (same as the solid line in the left plot). The change in zero point in the I-band, for example, is 0.04 mag. Also, for the I-band, the observed dispersion decreased considerably, from 0.37 mag down to 0.32 mag. For the B-band relation, it changed significantly as well from 0.45 to 0.41 mag. The dispersion remains unchanged when kinematical inclination angles are substituted for all other galaxies, indicating that the photometric determination of inclination angles for barred

galaxies are systematically different from the kinematical estimates.

Two possible explanations for the significant difference in the measured photometric and kinematical inclination angles of barred galaxies. The first is that the star formation rate is higher in the barred galaxies, although observations suggest that the effect of a bar on the disk star formation rate is unimportant (Kennicutt 1999). In Figure 5, colors of the calibrator galaxies are shown as a function of linewidth. The barred galaxies are indicated by open circles. In the plots on the left side, the photometric inclination angles were used to derive the corrected magnitudes, while on the right side, the magnitudes were corrected using the kinematical inclination angles for seven barred galaxies. Although most barred galaxies lie on the blue edge of this correlation if the photometric inclination angles are used (with one exception, NGC 3351, which is located at the red edge), when the kinematical inclination angles are substituted for barred galaxies, there are no longer any obvious differences between the distributions of the barred and non–barred galaxies. If an additional star formation is actually triggered by the presence of a bar, then one would expect the deviation of barred galaxies from the TF relation would be higher for shorter wavelength. We do not see such evidence, although our sample is rather small. We find the deviations from the mean TF fit for barred galaxies are the same for all five wavelengths. The second explanation, which is more plausible, is that the inclination angles for barred galaxies are over–estimated if the photometric inclination angles are used. This would make the barred galaxies appear brighter for a given linewidth, and would explain that adopting the kinematical inclination angles would shift these galaxies closer to the TF relation.

As stated in Section 2.2.2, in the following analysis in this paper, we will not use the kinematical inclination angles, because those for the I-band cluster survey galaxies were derived strictly from the photometric observations. In Figure 6, we show a TF relation for cluster galaxies. Those classified as barred are shown by solid circles. There is no obvious systematic offset between the barred and non–barred samples here, although one would expect that both the morphology identification and inclination estimates might be more difficult for distant galaxies. We have also examined the distribution of the ratio of number of barred to non–barred galaxies as a function of linewidth or inclination, but observed no significant difference between the cluster and calibrator samples.

## 4. APPLICATION OF THE TULLY–FISHER RELATION TO DISTANT CLUSTER SAMPLES AND THE VALUE OF THE HUBBLE CONSTANT

There have been numerous Tully–Fisher surveys of clusters of galaxies in various wavelengths. Most recently, Giovanelli and collaborators presented a survey of I-band photometry and radio linewidths of  $\sim 2000$  spiral galaxies in clusters out to  $\sim 10,000 \text{ km s}^{-1}$ . Aaronson, Huchra, Mould and collaborators presented H-band aperture magnitudes and 20% linewidths of galaxies in clusters out to  $\sim 15,000 \text{ km s}^{-1}$  (Aaronson et al. 1980, 1982, 1986 : hereafter AHM). Bothun et al. (1985) presented a catalog of  $UBVR$  multi-aperture photometry, H-band photometry and 21cm HI observations for several hundred spiral galaxies in 10 clusters. Han and Mould (1990) published I-band magnitudes for galaxies in the AHM survey. In this paper, we focus on the I-band survey by Giovanelli et al. (1997a), as it is the most complete one to date, and presents total I-band magnitudes measured from CCD observations, unlike in other

surveys where aperture magnitudes were used.

#### 4.1. *I*-band Cluster Distances and the Hubble Constant

The absolute calibration of the  $BVRIH_{-0.5}$  Tully–Fisher relations was presented in the previous section. The *I*-band relation was also re-calibrated for specific application to the G97 database. The second *I*-band calibration can now be applied to the distant cluster surveys, which extend out to  $\sim 10,000$  km s $^{-1}$ , to determine  $H_0$ .

For a detailed description of the *I*-band database, readers are referred to Giovanelli et al. (1997a) who explain in detail the selection criteria and the cluster galaxy membership. Briefly, the G97 survey is comprised of clusters and groups of galaxies out to 9000 km s $^{-1}$ . The database consists of 50% linewidths, total *I*-band magnitudes which were extrapolated to infinity (the largest isophotal ellipses measured were usually  $\sim 24.5$  mag arcsec $^{-2}$ ), and photometric inclination angles measured from *I*-band images.

In Table 3, we summarize the clusters of galaxies that are used in the following analyses to measure the Hubble constant. Also listed in this Table are three velocities for each cluster: velocities corrected for the Local Group frame, cosmic microwave background frame (CMB), and corrected for the flow model which will be described in Section 5.8.

To be included in the TF analyses, the galaxies had to meet all of the following criteria:

(1) They do not deviate by more than twice the dispersion from the TF relation. Three galaxies were excluded due to this: I1830 in the Fornax cluster, N2535 in Cancer, and N3832 in A1367.

(2) Galaxies must not be nearly face-on ( $i \leq 40^\circ$ ) because for these objects, the inclination uncertainty and subsequently the linewidth uncertainty is too large. Also, galaxies should not be close to edge-on ( $i \geq 80^\circ$ ) since the extinction correction for these become unreasonably large.

(3) The linewidth distribution of galaxies in the clusters should be similar to that of the calibrators. In Figure 7, some examples of clusters are shown. In the same figure, the calibrator data are over-plotted on each cluster TF relation with solid circles. The local calibrators and the cluster samples do not all cover the same rotational velocity range. For some clusters, such as Eridanus, Cancer, or Pegasus groups, the cluster sample extends to much smaller linewidths. In order to make a consistent sampling between the two sets of datasets, we apply a lower  $\log W$  cutoff of 2.35.

(4) The internal extinction correction should not exceed 0.6 mag. In Figure 8, the distributions of internal extinction values for the cluster galaxies and calibrators are obtained using three separate extinction corrections, that of T98, Han and Giovanelli et al. (see Appendix A for the latter two corrections). For the T98 and Giovanelli et al. corrections, there is a significant difference between the two samples: the cluster galaxies seem to have a long upper-end tail in their distribution of extinction values. To make a consistent sampling between the calibrators and clusters, we apply an upper cutoff of  $A_{int,I} = 0.6$  mag. It is also a matter of common sense to exclude galaxies more than half of whose light is obscured ( $A_{int} > 0.75$  mag).

The final *I*-band sample, referred to as the G97 sample, thus consists of 276 galaxies.

We measured the TF distances to all the clusters with 5 member galaxies or more by applying Equation 11 to the *I*-band survey. The results are shown in Tables 4 in which the cluster or group distances,  $D$ , and  $V/D$  values (corresponding to the ve-

locities with respect to the Local Group, CMB and model) are listed for *I*-band clusters. The uncertainty in the  $H_0$  values is roughly a combination of observational errors, errors in the TF zero points and slopes, and the dispersion of the TF relation. This will be discussed in more detail in Section 6.

The top plot in Figure 9 shows the Hubble diagram for the *I*-band clusters. Also in the bottom of the same figure, we plot the Hubble constant for each cluster as a function of velocity. In order to measure the values of  $H_0$ , we use only those clusters satisfying (1)  $V_{CMB} \geq 2000$  km s $^{-1}$ , and (2) velocities with respect to the CMB and the flow field model are within 10% of each other. This leaves us with a set of 15 clusters and groups of galaxies. Also, it will be shown in Section 5.1.2 that there are no selection biases for galaxies with  $V_{CMB} \geq 2000$  km s $^{-1}$ , thus using those clusters with  $V_{CMB} \geq 2000$  km s $^{-1}$  should be a reasonable choice. Taking an average of 15 clusters, we obtain  $H_0 = 73 \pm 2$  (random)  $\pm 9$  (systematic) using the *I*-band survey. The random and systematic errors are discussed in detail in Section 6.

#### 4.2. Comparison with Other Surveys

As mentioned above, there are other surveys of clusters of galaxies that reach velocities  $\sim 10,000$  km s $^{-1}$ , which are suitable for the determination of  $H_0$ . The G97 survey was used as the primary survey in this paper because of its completeness and quality. In this section, we compare our *I*-band  $H_0$  results with the distances and values of  $H_0$  obtained using other surveys.

##### 4.2.1. *H*-band

The *H*-band cluster surveys come from two sources: Aaronson et al. (1982) and Aaronson et al. (1986). We refer to the combined sample as AHM. In these surveys, rotational velocities were measured at the 20% level, and *H*-band aperture magnitudes were corrected to an isophotal aperture of  $\log A/D_1 = -0.5$  by adopting the system of the RC2 catalog (de Vaucouleurs, de Vaucouleurs, and Corwin 1976). These magnitudes are referred to as  $H_{-0.5}$  (see Aaronson, Mould and Huchra 1980 for details of how the interpolation was made). Also, in the original database of Aaronson et al. (1980), they included a  $3^\circ$  additive term for inclination angles. We are not adopting this convention, because we use the axis ratios given by RC3 catalog.

Cluster membership in the *H*-band survey was not as well defined as for the *I*-band survey, where G97 thoroughly inspected each cluster to determine which galaxies are likely members of the cluster. We examined the distribution of galaxies in each cluster in both spatial and velocity space to identify any outliers. Several clusters, including A1367, Z74–23, Hercules and Pegasus, were split into two or three subgroups.

The same four criteria listed above for the selection of the *I*-band survey galaxies are applied to the *H*-band AHM surveys. Again, to make the cluster database consistent with the calibrators, a lower cutoff of  $\log W \geq 2.35$  is applied. The final *H*-band sample thus consists of 163 galaxies in 26 clusters.

Following the method described in Section 3.2, the *H*-band TF relation was derived using both the calibrators and the cluster data. The resulting value of  $H_0$  is  $67 \pm 3$  (random)  $\pm 10$  (systematic). The 10% discrepancy between the *H*-band and *I*-band values of  $H_0$  is statistically significant, greater than the  $2\sigma$  level. Tormen & Burstein (1995) published a list of isophotal *H* magnitudes for galaxies from the AHM survey, corrected using RC3 parameters. Substituting this set of data for both the calibrators and cluster galaxies yields the same value of  $H_0$ ; use



TABLE 3  
Clusters of Galaxies in the I-band Survey

Cluster/ Group	R.A. <sup>a</sup> hh mm ss	DEC <sup>a</sup> dd mm ss	$V_{LG}$ km s <sup>-1</sup>	$V_{CMB}$ km s <sup>-1</sup>	$V_{Model}$ km s <sup>-1</sup>	N
N383	01 04 30	+32 12 00	5425	4924	5086	23
N507	01 20 00	+33 04 00	5350	5869	5016	14
A262	01 49 50	+35 54 40	5170	4730	4852	32
A400	02 55 00	+05 50 00	7258	7016	6983	26
Eridanus	03 30 00	-21 30 00	1641	1607	1627	35
Formax	03 36 34	-35 36 42	1328	1380	1372	44
Cancer	08 17 30	+21 14 00	4652	4982	4942	29
Antlia	10 27 45	-35 04 11	2505	3106	2821	26
Hydra	10 34 28	-27 16 26	3454	4061	3881	27
N3557	11 07 35	-37 16 00	2702	3294	2957	12
A1367	11 41 54	+20 07 00	6316	6709	6845	38
Ursa Major	11 54 00	+48 53 00	957	1088	1088	30
Cen30	12 46 06	-41 02 00	2756	3272	4445	39
Cen45	12 47 57	-40 22 23	4304	4820	4408	9
Coma	12 57 24	+28 15 00	6889	7143	7392	41
ESO508	13 09 54	-23 08 54	2662	3149	2896	17
A3574	13 46 06	-30 09 00	4308	4749	4617	20
Pavo	20 13 00	-71 00 00	3919	4027	4220	10
MDL59	22 00 18	-32 14 00	2621	2304	2664	26
Pegasus	23 17 43	+07 55 57	4109	3545	3874	19
A2634	23 35 55	+26 44 19	9516	8930	9142	27

<sup>a</sup>Positions given in Epoch 1950.0.

TABLE 4  
I-band Tully-Fisher Distances to Clusters

Cluster	N	$m-M$ (mag)	D (Mpc)	$V_{LG}/D$ (km/s/Mpc)	$V_{CMB}/D$ (km/s/Mpc)	$V_{model}/D$ (km/s/Mpc)
A1367	28	34.84	93.0	67.9 (11.0)	72.2 (11.7)	73.6 (11.9)
A2197	3	35.56	129.3	71.8 (11.4)	70.5 (11.1)	73.9 (11.7)
A262	22	34.18	68.7	75.3 (12.2)	68.9 (11.1)	74.2 (12.0)
A2634	20	35.36	118.0	80.6 (12.6)	75.7 (11.8)	77.5 (12.1)
A3574	14	34.03	64.1	67.2 (10.5)	74.1 (11.6)	72.0 (11.2)
A400	18	34.81	91.8	79.1 (12.3)	76.5 (11.9)	76.1 (11.8)
Antlia	16	33.30	45.6	54.9 ( 8.8)	68.1 (10.9)	61.8 ( 9.9)
Cancer	17	34.40	75.8	61.4 ( 9.8)	65.8 (10.5)	65.2 (10.4)
Cen30	22	33.25	44.7	61.7 (10.2)	73.2 (12.1)	99.5 (16.4)
Cen45	8	34.24	70.5	61.1 (10.0)	68.4 (11.2)	62.5 (10.3)
Coma	28	34.74	88.6	77.7 (12.2)	80.6 (12.6)	83.4 (13.0)
Eridanus	14	31.66	21.5	76.4 (12.4)	74.8 (12.1)	75.8 (12.3)
ESO508	9	33.07	41.1	64.8 (10.3)	76.7 (12.1)	70.5 (11.2)
Formax	14	30.93	15.3	86.6 (14.0)	90.0 (14.5)	89.5 (14.4)
Hydra	17	33.90	60.2	57.4 ( 8.9)	67.4 (10.5)	64.5 (10.0)
MDL59	10	32.56	32.5	80.7 (12.6)	71.0 (11.1)	82.1 (12.8)
N3557	9	33.02	40.2	67.2 (11.1)	81.9 (13.5)	73.5 (12.1)
N383	15	34.19	68.9	78.7 (12.3)	71.5 (11.2)	77.3 (12.1)
N507	7	33.86	59.1	90.6 (14.0)	82.4 (12.8)	89.0 (13.8)
Pavo	5	32.71	34.8	112.6 (17.4)	115.7 (17.9)	121.3 (18.7)
Pavo2	13	33.62	52.9	81.3 (13.0)	83.2 (13.4)	87.9 (14.1)
Pegasus	14	33.73	55.8	73.6 (11.5)	63.5 ( 9.9)	69.4 (10.9)
Ursa-Major	16	31.58	20.7	46.3 ( 7.1)	52.6 ( 8.1)	52.6 ( 8.1)

of these updated magnitudes does not reconcile the disagreement between I-band and H-band  $H_0$  values. We defer further discussion of this discrepancy to Section 4.2.3.

#### 4.2.2. B- and V-band Surveys

Bothun et al. (1985; hereafter B85) presented a catalog of 21cm HI observations, *UBVR* multi-aperture photometry, and H-band photometry of several hundred galaxies in 10 clusters. The total *UBVR* magnitudes were extracted from multiple-aperture measurements by applying the aperture corrections estimated from the mean growth curve derived from the RC2. The average aperture correction amounted to 0.2–0.3 mag. Of these 10 clusters, we selected five clusters, A1367, A400, A539, Coma and Z74–23, which consisted of at least five galaxies with good quality radio and optical data. Using 57 galaxies with  $\log W_{20} \geq 2.4$  in five clusters, we obtain  $H_0 = 80 \pm 8 \text{ km s}^{-1} \text{ Mpc}^{-1}$  (random) for B-band, and  $H_0 = 73 \pm 6 \text{ km s}^{-1} \text{ Mpc}^{-1}$  (random) for V-band. However, we note that the  $H_0$  value for A 539 is almost  $3\sigma$  larger than those of other four clusters, in both B-band and V-band estimates. Excluding this cluster, we obtain  $H_0 = 72 \pm 2 \text{ km s}^{-1} \text{ Mpc}^{-1}$  for B-band and  $68 \pm 2 \text{ km s}^{-1} \text{ Mpc}^{-1}$  for V-band. These values lie between the I-band and H-band results. We would put less weight on the B-band and V-band magnitudes as they were extrapolated from aperture magnitudes, and our B- and V-band calibrator magnitudes were not derived in the exactly the same manner.

#### 4.2.3. Discussion

We have calculated  $H_0$  using clusters of galaxies in four wavelengths: B, V, I and  $H_{0.5}$ . The derived values of  $H_0$  vary from 67 up to  $73 \text{ km s}^{-1} \text{ Mpc}^{-1}$ . In this section, we focus on the difference between the I-band and H-band results which are based on more reliable databases, and are statistically better as the number of cluster galaxies used to derive the value of  $H_0$  is more than twice as large as those in the B- and V-band surveys. It appears that the H-band TF relation yields consistently larger distances. We examine the databases carefully with other available published data in order to understand the root of the  $H_0$  discrepancy.

**Linewidth:** The I-band analysis is based on a different linewidth set ( $W_{50}$ ) than the H-band analysis ( $W_{20}$ ), so we first tested whether the discrepancy in distances was caused by a subtle error in one of the linewidth sets. Because TF relations are steep, it is important to measure linewidths accurately. Bothun et al. (1985) presented both 50% and 20% linewidths, and the 50% widths agree well with the published values of the G97 sample:  $\langle W_{\text{Bothun}}/W_{\text{G97}} \rangle = 1.000 \pm 0.003$ . As noted in Section 2, we re-measured 20% and 50% linewidths for the local calibrators, and found that the  $W_{20}/W_{50}$  ratios are consistent with those in the cluster samples,  $W_{20}/W_{50} = 1.07 \pm 0.03$  and  $1.10 \pm 0.05$  respectively. Furthermore, a list of galaxies that are in both G97 and AHM samples was compiled. The mean  $W_{20}/W_{50}$  ratio of galaxies in the overlapping sample ( $W_{20}/W_{50} = 1.10 \pm 0.08$ ) again agrees well with the mean ratio of the local calibrators. We have also compiled a set of  $\sim 70$  galaxies which had both I-band and H-band magnitudes, and also 20% and 50% linewidths measured, and confirmed that the derived values of  $H_0$  are insensitive to whether 20% or 50% linewidths are used. Han & Mould (1992) presented an I-band TF survey that used 20% linewidths. As an additional check we repeated the entire analysis using the Han & Mould database. We obtained distances that are consistent with those derived above using the G97 sample. This leads us next to the various

tests to confirm the photometric quality of the cluster data and calibrators.

**Photometry:** We first tested the zero point of the G97 I-band magnitudes by comparing them to those published by Han & Mould (1992). There were 59 galaxies that overlapped in the two surveys: they agree within 0.01 mag in the mean. On the other hand, Peletier and Willner (1993) published  $H_{0.5}$  magnitudes for Ursa Major cluster galaxies. We found that these also agreed within  $1\sigma$  error with the AHM magnitudes. The  $R-I$  colors of the TF calibrator galaxies (whose magnitudes are given by Macri et al. 2000) agree well with those of normal spiral galaxies presented in de Jong (1998).

Maeder et al. (priv. comm.) show that the concentric aperture photometry of Aaronson et al is verified by recent 2MASS survey photometry. But the consistency between calibrators' and clusters' isophotal diameters, on which  $H_{0.5}$  magnitudes are based, is more problematic. Diameters on the RC2 and RC3 systems differ by 0.1 dex (Tormen & Burstein 1995), and, while this apparently applies both to calibrators and cluster galaxies, the absence of systematic differences of the same order (equivalent to 0.2 mag in  $H_{0.5}$ ) cannot be guaranteed without further work.

#### Color Distribution of Calibrators and Cluster Galaxies:

The results above suggest that the difference in I-band and H-band distances must reflect a systematic difference in measured  $I-H_{0.5}$  colors between the calibrator and cluster samples. In the top panel of Figure 10, the I-band and  $H_{0.5}$ -band TF distance moduli are compared. In the middle plot, the  $I-H_{0.5}$  color of the same galaxies is shown as a function of linewidth. The calibrators are also shown by solid circles. The most striking feature is that calibrators are redder compared to the cluster sample galaxies (see below), which is the most likely reason the H- and I-band TF distances disagree at a 10% level (top figure). Environmental effects could possibly explain this difference. However, as shown in the bottom plot of Figure 9, the B-I color distributions of the two sets do agree. Furthermore, the R-I color distributions do not show any inconsistency between the two sets. K-S tests indicate that the chance that the  $I-H_{0.5}$  color distributions of the cluster galaxies and the calibrators are consistent is less than half of those for other colors.

**Virgo and Ursa Major Clusters:** Another test that indicates the preference for the I-band results is to examine  $RIH_{0.5}$  TF distances to the Ursa-Major and Virgo clusters. Pierce and Tully (1988) published  $RI$  magnitudes of nearly 20 galaxies in each of Ursa-Major and Virgo clusters. Also  $H_{0.5}$  magnitudes are available from the AHM survey. We applied our calibrated  $BRI$  TF relations to these samples to determine the distances. The  $H_{0.5}$  magnitudes for these galaxies were taken from the AHM survey. For both clusters, we find that the  $H_{0.5}$  distances are systematically larger, by 0.15 mag, or 7–8% in linear distance.

From these comparisons, we tentatively conclude that the H-band TF distances tend to be overestimated and should be used with caution: that is, there is something systematically different about the  $H_{0.5}$  magnitudes of the nearby calibrators and distant cluster galaxies. The I-band distances are consistent with those of B-, V- and R-band results, and the H-band  $H_0$  is inconsistent with other  $H_0$  values by  $2-4\sigma$ . Although they may be less affected by extinction, the  $H_{0.5}$  magnitudes are dependent on isophotal diameter measurements and the concomitant aspect ratio corrections. There may be a systematic difference in  $H_{0.5}$  magnitudes of local calibrators and cluster galaxies. This will

require further investigation, but is beyond the scope of this paper, and the discrepancy is likely not solved without a consistent set of total H-band magnitudes. However, the measurement of total H magnitudes is made difficult by a sky background which is more than 100 times brighter at H than I, and needs to be correctly subtracted from the low surface brightness profiles in the outer parts of galaxies. Until better photometry than the current H database becomes available, the photometric systematics we have struck here may set the limits on  $H_0$  measurements from the Tully-Fisher study.

## 5. DISCUSSION

We have derived the value of  $H_0$  by focusing on the survey by G97 who presented the 21 cm linewidth and I-band photometry data for several hundred galaxies in clusters out to  $\sim 10,000$  km s $^{-1}$ . In the previous section, this value was then compared with other surveys of different wavelengths. In this Section, we discuss how biases and systematic uncertainties can affect the value of  $H_0$ , concentrating on the I-band database.

### 5.1. Biases

#### 5.1.1. Consistency between the Calibration and Distant Galaxies Samples

Not only do the local calibrators and cluster sample galaxies have to be on the same photometric and kinematical systems, they also need to be of similar type. The  $B-I$  color as a function of linewidth has often been used as this is a good indicator of the variations in the recent star formation rate ( $\sim 1$  Gyr). It is also sensitive to the internal extinction correction. Unfortunately for majority of the galaxies in the G97 I-band survey, there are no  $B$  magnitudes available. We thus compare our local calibrators with galaxies in the Virgo and Ursa Major clusters whose photometric and linewidth data have been published by Pierce & Tully (1988). These clusters should be representative of other clusters of galaxies that are used in the two all-sky surveys we are calibrating, especially since the spiral galaxies used are not located in the immediate centers of the clusters, but in the “infall” regions.

In Figure 10 (bottom), we showed the  $B-I$  color distributions of Virgo and Ursa-Major cluster galaxies as a function of linewidth. The local calibrators were over-plotted by solid circles. The two cluster samples – Virgo and Ursa Major – show no significant difference between their galaxy populations. Furthermore, we see no significant difference between the local calibrator sample and the two clusters. This was not the case when Pierce & Tully (1988) first examined this diagram; they reported that six local calibrator galaxies from their sample were found systematically on the blue edge of this color–linewidth relation. The enlarged sample here indicates that there is no systematic difference between the local calibrators and cluster galaxy samples.

Another important issue that needs to be addressed is the difference in environment between the calibration and cluster galaxies. Of 21 calibrators, only seven are members of well defined groups/clusters of galaxies: the Virgo, Fornax, and Leo I clusters. The rest are members of loose groups or are field galaxies. The application of the TF calibration based on such a sample to the distant cluster data could potentially introduce another systematic uncertainty, as cluster and field galaxies could be inherently different. Using these seven calibrators only and fixing the slope to that obtained from the cluster data, we derived an I-band TF zero point (for a 50% linewidth relation) of

$-21.44 \pm 0.17$  mag. This agrees within  $1\sigma$  of the zero point obtained in Equation 11, suggesting that within our limited sample, there is no significant evidence for environmental dependence in TF relations. A more rigorous, statistically better defined analysis is presented by Giovanelli (1997b) who examined the I-band TF residuals for galaxies grouped by the projected radial distance from the center of clusters. They found no zero point offset between subsamples. In light of these results, we make no attempt to separate the field galaxies from the cluster galaxies in the calibration.

#### 5.1.2. Selection Biases in the I-band

In measuring the Hubble constant using distant cluster data, it is important to account correctly for selection effects which include the Malmquist bias and cluster population incompleteness bias. The former arises in field surveys, for example, where galaxies are distributed uniformly and thus there are more galaxies per unit volume at larger distances. If each true distance is scattered randomly, then more galaxies are scattered “downward” (i.e. smaller distances) than “upward”. Thus, the distances are underestimated. This type of bias was first examined in detail by Lynden-Bell et al. (1988). Later, several authors expanded on this subject, including Gould (1993), Landy & Szalay (1992) and Willick (1994). As for the cluster population incompleteness bias (CPIB), if not properly corrected for, the clusters would appear brighter than they actually are because only the brightest galaxies in them are observed in a flux-limited sample, leading to a biased value of the Hubble constant.

There are numerous theoretical and empirical studies that have dealt with the CPIB. Teerikorpi, Bottinelli and collaborators introduced a quantitative approach to this problem (Teerikorpi 1984, 1987, Bottinelli et al. 1988). Willick (1994) also presented a more extensive quantitative analysis of the statistical bias. We will show in this section using the formalism presented by G97 that the CPIB in our sample is small, affecting the derived value of the  $H_0$  by less than 5%.

Federspiel et al. (1994, hereafter FST94) investigated the bias properties of the TF distances using a field sample of 1355 galaxies from the Mathewson–Ford–Buchhorn survey. One of the main conclusions presented by that study was that in a flux-limited sample, at a given redshift (which is to first order, distance), the Hubble constant is multi-valued for different values of rotational velocity and apparent magnitude. The trend is that for galaxies with similar rotational velocities, the Hubble constant rises as the redshift becomes larger, and for a given redshift, a higher  $H_0$  is found for smaller galaxies (smaller rotational velocities) (for details, see Figures 1 and 2 of FST94). They also showed that the zero point of the TF relation is sensitive to the redshift, and to apparent magnitude as well. Such biases clearly need to be corrected for if field samples are to be used to measure the Hubble constant.

We show, however, that for our cluster samples of the I-band spiral galaxies, these biases are small. Here, we examine the two distant cluster surveys which we are calibrating to measure  $H_0$ , to see to what extent they may be affected by the incompleteness biases discussed by FST94.

In Figure 11, I-band TF relations are shown for the G97 cluster sample. Absolute magnitudes were calculated assuming  $H_0 = 100$  km s $^{-1}$  Mpc $^{-1}$  and that velocities (in the CMB reference frame) give distances to first order. The choice of  $H_0$  here is not critical, as we are interested in examining the *relative* offsets of different subsamples. In the left panel of Figure

10, subgroups are divided by their velocities, and the mean of each bin is shown. With the exception of the nearest sample ( $cz < 2000 \text{ km s}^{-1}$ ), there is no significant difference among the subsamples. The slight offset in the zero point of the nearest sample is most likely due to its complex velocity field not being characterized effectively by the CMB reference frame. The right panel of Figure 10 shows subgroups divided by apparent magnitudes. If the I-band TF sample is being severely affected by its flux limit, then we should observe a systematic trend in the zero points of the subsamples. That is not the case, however. The four subsamples, although some suffer from small number statistics, show no significant dependence of TF zero point on the apparent magnitude.

Lack of selection biases suggests that the incompleteness bias in the G97 I-band sample is not severe, especially if the TF sample is restricted, for example to those galaxies with larger rotational velocities ( $\log W > 2.35$  – see Figure 7). In the next subsection (5.1.3), we will show quantitatively that cluster population incompleteness bias for our cluster samples is at most 0.03–0.05 mag, or 1–2% in distance, and hence in the value of  $H_0$ .

### 5.1.3. Cluster Population Incompleteness Bias

We showed in the previous section that the selection bias with respect to apparent magnitude or redshift is negligible. In this section, we take a more quantitative approach to correct for selection biases.

There are several approaches to correct for CPIB. Giovanelli et al. (1997b) presented a thorough, comprehensive method to correct for this bias, which we apply to the I-band survey. The basic idea is that the observed luminosity function for each cluster is compared with the expected one derived from a theoretical luminosity function such as the Schechter function. Then a random sample is drawn from the model to represent the observed cluster. After 1000 iterations, the zero point of the TF relation obtained from the simulated sample is compared to that of the observed one, to estimate the bias. The detailed description of this CPIB method is found in Giovanelli et al. (1997b).

The cluster population incompleteness bias amounts to, on the average,  $\sim 0.03$ – $0.05$  mag, corresponding to  $\sim 1$ – $2\%$  in distance. Unlike what some authors have claimed in the past (e.g. Sandage, Tammann and collaborators), incompleteness bias is almost negligible. For example, Sandage (1994) had suggested that one of the reasons that the TF method gave a high Hubble constant value was because only the brightest galaxies in the cluster were observed: in particular, he believed that only the “upper” half of the TF relation was being considered. This is not what is actually happening. These simulations show that the galaxies with  $\log W \geq 2.5$  are virtually unaffected by the cluster population incompleteness bias. Thus the overall bias per cluster amounts to only a couple of percent in distance.

## 5.2. Systematic Uncertainties in $H_0$

It is important to address how systematic uncertainties can affect  $H_0$ . In this section, we focus on the following: (1) the slope and shape of the TF relation, concentrating on how much a use of a wrong slope value can affect the  $H_0$ , and also whether the application of quadratic fits would significantly change the  $H_0$  values; (2) the metallicity dependence of the Cepheid period–luminosity relation; (3) the internal extinction correction method used; and (4) velocity flow field models, focusing on how dependent the value of  $H_0$  is on the velocity

reference frame adopted. Table 5 summarizes all the values of  $H_0$  derived for each test, details of which are described below.

### 5.2.1. Dependence of $H_0$ on TF Slope and Shape

The effect of slope uncertainties on the value of  $H_0$  is small. We estimated the Hubble constant with three different assumptions for the I-band slope of  $-9.00$ ,  $-10.00$ , and  $-11.00$ . We obtain  $75 \pm 4$ ,  $73 \pm 2$ , and  $71 \pm 2 \text{ km s}^{-1} \text{ Mpc}^{-1}$  respectively. Errors quoted here include only the random uncertainties. In this exercise, we changed the value of the slope by 1.0; in reality, this corresponds to more than  $10\sigma$ , which suggests that a use of incorrect TF slope will affect  $H_0$  insignificantly, perhaps 2–3% at most.

In Appendix C, quadratic TF relations were derived for each wavelength. To demonstrate that the changes in the shape of the TF relation affects  $H_0$  very little, we applied the quadratic equation to the I-band cluster data. Note that the equation (C4) was derived for 20% linewidth. Here, we used a similar relation derived for the 50% linewidth. This yielded  $H_0 = 73 \pm 2 \text{ km s}^{-1} \text{ Mpc}^{-1}$ .

### 5.2.2. Effects of Metallicity Dependence of the Cepheid PL Relation on $H_0$

Whether the Cepheid period–luminosity relation depends on the metallicity of the Cepheid variable stars has been a particularly important concern for the  $H_0$  HST Key Project. It may be one of the larger sources of systematic errors in the Cepheid distance scale. The metallicities of the Key Project galaxies vary almost by an order of magnitude. All the distances have been determined with respect to that of the LMC, for which we adopt  $(m - M)_0 = 18.50 \pm 0.13$  mag. However, the metal abundances of the TF calibrators cover a wide range, up to five times higher than LMC. Several observational and theoretical studies claim to have constrained this metallicity effect (see Kennicutt et al. 1998). Some estimates suggested a dependence of as much as 0.8 magnitude per factor of 10 increase in abundance (e.g. Gould 1994). Because most of the galaxies used in our TF calibration are more metal rich than the LMC, if such a steep dependence indeed existed, it could potentially modify the TF zero points significantly, and hence the derived value of  $H_0$ .

We have re-derived TF relations using the metallicity dependence of  $\gamma = \delta(m - M)_0 / \delta[O/H] = -0.24 \pm 0.16 \text{ mag/dex}$ , derived from the differential test of Cepheid distances to two fields in M 101 (Kennicutt et al. 1998). Figure 12 shows the I-band TF relation without corrections for the metallicity dependence of Cepheid PL relation (solid circles) and with corrections (open circles). The metallicity-corrected set of  $BVR_{I,H-0.5}$  TF relations are:

$$B_{T,Z}^c = -8.02(\pm 0.72)(\log W_{20}^c - 2.5) - 19.78(\pm 0.11) \quad (12)$$

$$V_{T,Z}^c = -9.00(\pm 0.83)(\log W_{20}^c - 2.5) - 20.34(\pm 0.12) \quad (13)$$

$$R_{T,Z}^c = -8.89(\pm 0.72)(\log W_{20}^c - 2.5) - 20.67(\pm 0.11) \quad (14)$$

$$I_{T,Z}^c = -9.42(\pm 0.76)(\log W_{20}^c - 2.5) - 21.15(\pm 0.12) \quad (15)$$

$$H_{-0.5,Z}^c = -11.21(\pm 0.87)(\log W_{20}^c - 2.5) - 21.80(\pm 0.14) \quad (16)$$

We have also re-derived the I-band TF relation using the second calibration method which was actually applied to the distant clusters to derive  $H_0$ . This method incorporated the cluster galaxy data, using the 50% linewidths:

$$I_{T,Z}^c = -10.00(\pm 0.12)(\log W_{50}^c - 2.5) - 21.41 \quad (17)$$

TABLE 5  
Systematic Errors affecting the I–band  $H_0$

Errors	$H_0$	Errors	$H_0$
<i>TF Slope</i>		<i>Extinction Correction</i>	
–11.00	$71 \pm 2$	T98	$73 \pm 2$
–10.00	$73 \pm 2$	Giovanelli et al.	$74 \pm 2$
–9.00	$75 \pm 2$	Han	$73 \pm 1$
Quadratic Fits	$73 \pm 2$	<i>Velocity Models</i>	
With Metallicity Correction	$70 \pm 2$	Local Group	$71 \pm 3$
Without Metallicity Correction	$73 \pm 2$	CMB	$73 \pm 2$
		Infall Model	$74 \pm 3$

\*Unless otherwise indicated, the velocities in the CMB reference frame were used.

The metallicity–corrected zero points above are brighter, as most of the galaxies in this particular sample are more metal rich than the LMC. Following the same exercise shown in Section 3.2, we have calculated the TF zero point by adopting the slope measured from the cluster galaxies. The value of  $H_0$  derived using the Cepheid distances corrected for their metallicity dependence is  $H_0 = 70 \pm 2 \text{ km s}^{-1} \text{ Mpc}^{-1}$ ,  $\sim 4\%$  smaller than one obtained without any corrections.

### 5.2.3. Effects of the Uncertainties in the Adopted Internal Extinction Corrections on $H_0$

One of the largest corrections applied to the raw magnitudes is the internal extinction correction, for which we adopted the expressions derived by T98. The internal extinction for highly inclined galaxies amounts to more than 0.5 mag. In Table A1 (in Appendix A), we listed values of internal extinction for each Cepheid calibrator galaxy determined via three separate methods: Tully et al. (1998), Giovanelli et al. (1994) and Han (1992). The large dispersion between these methods suggests that the internal extinction corrections are not being determined uniquely. Can the choice of extinction correction method affect the measured value of  $H_0$ ?

To quantify such an effect, we derived  $H_0$  using all three above methods of internal extinction correction. For each set of calculations, magnitudes of both calibrator and cluster galaxies are treated using the same corrections for consistency, then the slope and zero point of the I–band TF relation are estimated, as is the incompleteness bias for each cluster, and finally  $H_0$  is calculated from the measurements of TF distances to the clusters. For three extinction correction methods, T98, Giovanelli’s and Han’s, we obtain  $H_0 = 73 \pm 2$ ,  $74 \pm 2$  and  $73 \pm 1 \text{ km s}^{-1} \text{ Mpc}^{-1}$  respectively. As we had expected,  $H_0$  is virtually insensitive to the extinction correction method used.

Furthermore, there is of course the inclination uncertainty which propagates through the extinction correction eventually to the error in  $H_0$ . A full error analysis is provided in the next section.

### 5.2.4. Dependence of $H_0$ on the Large–Scale Velocity Field

One of the major remaining uncertainties in the determination of the  $H_0$  is the correction of the observed velocities of galaxy clusters for large–scale peculiar motions. It is now clear that there are motions on scales of tens of Mpc’s with amplitudes up to few hundreds of  $\text{km s}^{-1}$  with respect to the CMB.

However, the exact nature of these motions is still unclear (Lauer and Postman 1994; Riess, Press and Kirshner 1995), especially in terms of what precisely are the causes of these motions. In Table 3, we listed three velocities: with respect to the Local Group reference frame, CMB frame, and the modeled flow field, all of which were used to derive  $H_0$  for each cluster for I–band surveys. The observed heliocentric velocity ( $V_H$ ) of the galaxies are corrected to the centroid of the Local Group following Yahil, Tammann and Sandage (1977), and also to the CMB frame via the relation from Giovanelli et al. (1998). The flow field model adopted in this paper is a multi–attractor model which included the Virgo cluster, the Great Attractor and the Shapley concentration. The details of the flow field model are presented in Mould et al. (1999).

The flow field model is explained briefly as follows. It is a multi–attractor linear model based on Han and Mould (1990) and Han (1992). The model is comprised of three attractors: (1) the Virgo cluster at  $(\text{RA}, \text{DEC}, V_H) = (12.472h, +12^\circ 67', 1035 \text{ km s}^{-1})$ , with an assumed radius of 10 degrees; (2) the Great Attractor at  $(13.333h, -44^\circ 00', 4600 \text{ km s}^{-1})$ , with an assumed radius of 10 degrees; and (3) the Shapley concentration at  $(13.50h, -31^\circ 0', 13800 \text{ km s}^{-1})$ , with a radius of 12 degrees. The flows toward each attractor are assumed to be independent of each other, thus the total velocity correction is a vector sum of all three peculiar motions.

As shown in Table 5 in which we have listed  $H_0$  estimates using three different velocities,  $H_0$  is not sensitive to the velocity field adopted. The value of  $H_0$  remains unchanged whether we adopt the velocities in the CMB frame of reference or those derived using the infall model.

## 6. UNCERTAINTY IN THE HUBBLE CONSTANT

Understanding all the sources of errors, both systematic and random, and how they propagate into the uncertainty in the value of the Hubble constant is almost as challenging as the actual measurement of  $H_0$  itself. Table 6 shows how the uncertainty in  $H_0$  is derived. Here, we focus on the derivation of uncertainties for the I–band survey, as that for the other surveys should be similar.

The first part describes the errors in the Cepheid distance scale. Much of this has been discussed in detail in previous

papers of this series. The largest systematic error originates in the uncertainty of the distance to LMC, with respect to which all of the Cepheid distances have been measured. Combining the LMC distance uncertainty with other errors such as those in the HST photometric zero points, extinction treatment and in the photometry of Cepheid variables themselves, the total random and systematic errors of the Cepheid distance scale add up to 0.08 and 0.16 mag respectively.

Next, the uncertainties in the TF distance scale are considered. Using simulations, we have determined that the errors in the zero points and slopes of the TF relations are 0.09 and 0.13 mag respectively. For the H–band TF relation, however, we assign a larger error for its zero point (0.25 mag) because of the systematic uncertainties in the photometry of galaxies between the calibrator and cluster samples. This was discussed in Section 4.2. A typical error in the measured apparent magnitude of cluster galaxies is  $\sim 0.04$  mag. We have also assigned a typical error of  $15 \text{ km s}^{-1}$  to the linewidth measurements, which is a conservative estimate. For a typical galaxy in our sample with  $\log W \simeq 2.6$ , a  $15 \text{ km s}^{-1}$  error is equivalent to 0.04 mag. There is in addition an uncertainty of 0.04 mag in the internal extinction correction, which was estimated from comparing three different correction methods (Appendix A). Furthermore, the Galactic reddening adds an uncertainty of 0.02 mag. These uncertainties, however, are reduced by the number of target galaxies in each cluster,  $\sqrt{n}$ . Thus the total random error in the TF magnitudes per cluster is only 0.03 mag, assuming a typical number of galaxies per cluster of 16. The total linewidth error is 0.01 mag, again assuming  $n = 16$ .

We learned in Section 3.4 that the intrinsic dispersion of the TF relation is  $\sim 0.20$ – $0.25$  mag. Again, the uncertainty in the TF cluster distance due to the intrinsic dispersion is reduced by a factor  $\sqrt{n}$ . The total random error in the TF distance moduli is therefore the photometric error, the linewidth error multiplied by the slope, and the intrinsic dispersion combined in quadrature. Note that we have excluded the error in the TF slope. We have shown in Section 5.2.1 that the slope uncertainty has a negligible effect on the value of  $H_0$ .

The total systematic error in the TF distance modulus consists of three terms. The first is the error in the TF zero point calibration, which we estimated to be 0.09 mag using Monte–Carlo simulations. Another term is the systematic uncertainty arising from the internal extinction correction. We have excluded any galaxies that required an internal extinction correction of 0.6 mag or more, however, there still might be a slight systematic error due to the fact that the *mean* extinction corrections are not the same for the clusters and calibrators. We have included this uncertainty (0.04 mag) in the total systematic error of the TF distance moduli. Adding these two terms in quadrature with the systematic error of the Cepheid distance scale (0.16 mag), we estimate the total systematic error of the TF distance scale to be 0.22 mag.

Finally, the uncertainty in the value of  $H_0$  can be determined. In addition to the total random error on the TF distance moduli derived above, the random error of the cluster velocities needs to be considered. In the last section, it was shown that the value of  $H_0$  was affected by the velocity flow field adopted, due to uncertainties arising from not understanding fully what the sources of peculiar motions of clusters are, and also due to the non–uniform distribution of clusters with respect to the CMB dipole. Giovanelli et al. (1998) report that the distribution of peculiar velocities of clusters in the CMB reference frame has a dispersion of  $300 \text{ km s}^{-1}$ . We assign this  $300 \text{ km s}^{-1}$  as an

additional random uncertainty in the determination of the  $H_0$  value.

Combining all the errors, we obtain  $H_0 = 73 \pm 2 \pm 7$  in the I–band (the first and second uncertainties correspond to random and systematic respectively),  $72 \pm 2 \pm 11$  in the B–band,  $68 \pm 2 \pm 10$  in the V–band, and  $67 \pm 2 \pm 10$  in the H–band. Again, larger systematic errors for the H–band result are due to its less certain TF relation zero point. We have also adopted larger systematic errors for the B– and V–band results as for these, the photometric data for calibrator and cluster galaxies were not derived in a consistent manner, although both use total magnitudes. We take the weighted average of these four estimates to derive the value of the Hubble constant, where the weights are defined as the inverse square of the quadrature sum of the errors that are intrinsic to the TF relations. These include the random error on the TF moduli (R2.4 in Table 6), the systematic error on the TF zero point (S2.1), and the systematic error in the internal extinction correction (S2.2). In Table 6, the error estimates for the I–band TF relation were listed. For other wavelengths, the extinction correction uncertainties are scaled by 2.75 for B–band, 1.5 for V–band and 0.5 for H–band. Thus, the total random error on the TF moduli are 0.12 mag, 0.11 mag, 0.12 mag and 0.12 mag for B, V, I and H–band TF relations respectively. As indicated above, the systematic error on the TF zero point is 0.13 mag for the I–band, while for others, we have adopted 0.25 mag. The weighted value of the Hubble constant is therefore:

$$H_0 = 71 \pm 4 \text{ (random)} \pm 7 \text{ (systematic)} \text{ km s}^{-1} \text{ Mpc}^{-1}. \quad (18)$$

## 7. SUMMARY

The HST Key Project on Extragalactic Distance Scale has contributed enormously in building the cosmic distance scale. Taking the Tully–Fisher relation alone as an example, the number of its calibrators have quadrupled as a result of Cepheid observations using the HST. This significantly improved the accuracy of the TF relation zero point, and effectively the value of  $H_0$ . Furthermore, numerous all–sky surveys, such as the one we used in this paper by Giovanelli et al., allowed us to extend the galaxy distances far out enough such that their peculiar velocities are significantly small compared to their recession velocities.

In this paper, we have derived the value of the Hubble constant using the I–band Tully–Fisher relation. The BVR<sub>I</sub>H<sub>0.5</sub> TF relations were calibrated using ground–based photometry data from Macri et al. (2000) and Aaronson, Huchra and Mould (1982, 1986), and Cepheid distances published as part of the series in Papers I through XXIII of this series. These were then applied to the published cluster surveys of Giovanelli et al. (I–band), Bothun et al. (B–band and V–band), and Aaronson et al. (H–band) to derive the value of  $H_0$ . The clusters extend out to  $V_{\text{cmb}} \simeq 10,000 \text{ km s}^{-1}$ . Taking the weighted average of Hubble constants derived using four different surveys, we obtained  $H_0 = 71 \pm 4 \text{ (random)} \pm 7 \text{ (systematic)} \text{ km s}^{-1} \text{ Mpc}^{-1}$ .

Table 7 lists published  $H_0$  values derived using the TF relation. Focusing on the values published during past five years, the estimates vary from the low 50s to the low 80s. There are mainly three reasons for this variation. First is the calibration of the TF relation. Mould et al. (1996) showed that doubling the number of calibrators changed the zero point of the TF relation by nearly 0.3 mag, consequently lowering the value of  $H_0$  by 15%. Another example arises when comparing our I–band  $H_0$  value with that of Giovanelli (1997). As shown in Table 5,

TABLE 6  
Error Budget (I–band)

	Source	Error <sup>a</sup>	Notes
1.	<b>Cepheid Distance Scale</b>		
	A. LMC True Modulus	$\pm 0.13$	Adopted from Westerlund (1997)
	B. LMC PL Zero Point	$\pm 0.02$	From Madore & Freedman (1991)
S1.1	LMC PL Systematic Error	$\pm 0.13$	A and B added in quadrature
	D. HST V–Band Zero Point <sup>b</sup>	$\pm 0.03^b$	
	E. HST I–Band Zero Point <sup>b</sup>	$\pm 0.03^b$	
S1.2	Systematic Error in the Photometry	$\pm 0.09$	$\sqrt{D^2(1-R)^2 + E^2R^2}$ , $R = A(V)/E(V-I) = 2.45$
R1.1	Random Error in the Photometry	$\pm 0.05$	From DoPHOT/ALLFRAME comparison
	F. $R_V$ Differences Between Galaxy and LMC	$\pm 0.014$	See Ferrarese et al. 1998 for details
	G. Errors in the adopted value for $R_V$	$\pm 0.01$	See Ferrarese et al. 1998 for details
R1.2	Random Error in the Extinction Treatment	$\pm 0.02$	F and G added in quadrature
	H. PL Fit (V)	$\pm 0.05^c$	
	I. PL Fit (I)	$\pm 0.04^c$	
R1.3	Random Error in the Cepheid True Modulus <sup>d</sup>	$\pm 0.06^c$	H and I partially correlated
R <sub>PL</sub>	Total Random Error	$\pm 0.08$	R1.1, R1.2 and R1.3 added in quadrature
S <sub>PL</sub>	Total Systematic Error	$\pm 0.16$	S1.1 and S1.2 added in quadrature
2.	<b>Tully–Fisher Distance Scale</b>		
	A. Error in the measured apparent magnitude	$\pm 0.10^f/\sqrt{n}$	
	B. Error in the corrected linewidth	$\pm 0.04^g/\sqrt{n}$	
	C. Error in the internal extinction correction	$\pm 0.04^g/\sqrt{n}$	average value from Table A1
	D. Error in the Galactic reddening	$\pm 0.02$	Typical value given in §6
R2.1	Random Error in the TF Magnitudes	$\pm 0.03$	A, C and D added in quadrature with $n = 16$
R2.2	Random Error in the linewidth	$\pm 0.01$	$n$ assumed to be 16
R2.3	Intrinsic Dispersion of TF Relations	$\pm 0.20/\sqrt{n}$	
R2.4	Random Error on the TF moduli	$\pm 0.12$	$\sqrt{R2.1^2 + (10.0 \times R2.2)^2 + R2.3^2}$
S2.1	Systematic Error on the TF Zero Point	$\pm 0.13$	from Equation 9
S2.2	Systematic Error in the internal extinction correction	$\pm 0.04$	from Table A1 multiplied by $\Delta A_I$ (cluster - calibrators)
S2.3	Systematic Error due to the metallicity dependence of Cepheid distance scale	$\pm 0.08$	see Section 5.2.2
R <sub>TF</sub>	Total Random Error on the TF Distance Moduli	$\pm 0.12$	R2.4
S <sub>TF</sub>	Total Systematic Error on the TF Distance Moduli	$\pm 0.22$	S2.1, S2.2, S2.3, and S <sub>PL</sub> added in quadrature
3.	<b>Hubble Constant</b>		
R3.1	Random Error on the TF Cluster Velocities	$\pm 300^e$	in km/sec
R <sub>H<sub>0</sub></sub>	Total Random Error on $H_0$	$\pm 2$	$\sqrt{(R3.1/v)^2 + (0.46H_0R_{TF})^2}/\sqrt{N}$ , in km/sec <sup>g</sup>
S <sub>H<sub>0</sub></sub>	Total Systematic Error on $H_0$	$\pm 7$	$0.46H_0S_{TF}$ in km/sec/Mpc

<sup>a</sup>Errors are in magnitudes for sections 1 and 2, and as indicated for section 3.

<sup>b</sup>Contributing uncertainties from the Holtzman et al. (1995) zero points, and the long–versus short uncertainty, combined in quadrature.

<sup>c</sup>The values quoted are typical but individual cases vary slightly.

<sup>d</sup>The partially correlated nature of the derived PL width uncertainties is taken into account by the (correlated) de–reddening procedure, coupled with the largely ‘degenerate–with–reddening’ positioning of individual Cepheids within the instability strip.

<sup>e</sup>Giovanelli’s analysis of the velocity field.

<sup>f</sup>Each cluster is assumed to have  $n$  TF galaxies.

<sup>g</sup> $v = 5000$ km/s, and  $N$  clusters of galaxies are used to derive the  $H_0$ .

TABLE 7  
Estimates of  $H_0$  using Tully–Fisher Relation

$H_0$	Method <sup>a</sup>	Sample	Source
$50 \pm 4$	BTF	Virgo	Sandage & Tammann 1976
$80 \pm 8$	BTF	Virgo	Tully & Fisher, 1977
$76 \pm 8$	BTF	Virgo	Bottinelli & Gouguenheim 1977
$61 \pm 4$	IRTF	Virgo and Ursa Major	Aaronson, Mould & Huchra, 1979
$65 \pm 4$	IRTF	Virgo	Mould, Aaronson & Huchra, 1980
$95 \pm 4$	IRTF	4 clusters <6000 km/s	Aaronson et al. 1980
$63 \pm 10$	$(H - I)$ vs log $W$ relation	Virgo	Tully, Mould & Aaronson 1982
$71 \pm 2$	VTF,RTF,IVTF	Clusters <6,000 km/s	Visvanathan, 1982
$82 \pm 10$	BTF,IRTF	Groups <6000 km/s	Aaronson & Mould, 1983
$74 \pm 11$	VTF,RTF,IVTF	Clusters <6000 km/s	Visvanathan, 1983
$55 \pm 9$	IRTF	Coma tied to Virgo	Sandage & Tammann, 1984
$91 \pm 3$	IRTF	20 Sc I's <13,500 km/s	Bothun et al. 1984
$92 \pm 1$	IRTF	Clusters <11,000 km/s	Aaronson et al. 1986
$85 \pm 10$	B,R,IRTF	Virgo and Ursa Major	Pierce & Tully 1988
$57 \pm 1$	BTF, IRTF	Virgo	Kraan-Korteweg, Cameron & Tammann, 1988
$68 \pm 8$	BTF	Virgo	Fouque et al. 1990
$92^{+21}_{-17}$	BTF	Coma	Fukugita et al. 1991
$73 \pm 4$	IRTF	Clusters <11,000 km/s	Mould et al. 1996
$69 \pm 8$	IRTF	Virgo, Ursa–Major	Shanks 1997
$82 \pm 10$	BTF	Virgo	Yasuda, Fukugita & Okamura, 1997
$69 \pm 5$	ITF	Clusters <~10,000 km/s	Giovanelli et al. 1997a
$53 \pm 5$	BTF magnitudes	KLUN <sup>b</sup>	Theureau et al. 1997
$57 \pm 5$	BTF diameters	KLUN <sup>b</sup>	Theureau et al. 1997
$57 \pm 7$	BTF	Clusters <11,000 km/s tied to Virgo	Federspiel, Tammann & Sandage 1998
$56 \pm 3$	BTF	KLUN (HST Calibration)	Theureau 1998
$51 \pm 4$	BTF	KLUN (HIPPARCOS calibration)	Theureau 1998
$53 \pm 3$	BTF	Field galaxies <5000 km/s	Tammann 1999
$56 \pm 3$	BTF	Clusters <11,000 km/s tied to Virgo	Tammann 1999
$77 \pm 4$	ITF	Clusters <8,000 km/s	Tully 1999
$76 \pm 3$	ITF	Clusters <8000 km/s	Madore et al. 1999
$52 \pm 5$	BTF inverse diameter	KLUN	Ekholm et al. 1999
$53 \pm 6$	BTF inverse magnitude	KLUN	Ekholm et al. 1999

<sup>a</sup>ITF: I–band TF; IRTF: IR TF; BTF: B–band TF; VTF: V–band TF; RTF: R–band TF; IVTF: 10500Å

<sup>b</sup>KLUN stands for Kinematics of the Local Universe, which consists of a sample of 5171 spiral galaxies out to ~5000 km/s.



using Giovanelli et al's extinction correction method, and applying that to all the clusters (no velocity cutoff), we obtained  $H_0 = 76 \pm 3 \text{ km s}^{-1} \text{ Mpc}^{-1}$ , whereas Giovanelli (1997) reported  $H_0 = 70 \pm 5 \text{ km s}^{-1} \text{ Mpc}^{-1}$ . Even though these two values agree with each other within  $1\sigma$ , the difference is attributed to a different calibration. Giovanelli (1997) used a smaller sample of 11 galaxies, instead of 21 that we used in this paper. Using the calibrators of Giovanelli (1997), we do in fact retrieve the same  $H_0$  value. Increasing the number of calibrators again by 70% (from 11 to 19) contributes considerably to the change in the value of  $H_0$ . Furthermore, the same argument applies for the difference between the values of  $H_0$  obtained by Aaronson et al (1980) and this paper which used the same set of clusters. The calibration adopted by the former consisted only of two galaxies, M31 and M33. The decrease in  $H_0$  is almost entirely due to the fact that these two galaxies lie well below the TF relation, thereby systematically yielding a lower  $H_0$  value.

The second reason behind the various inconsistent estimates is the treatment of the cluster population incompleteness bias. Sandage, Tammann, Federspiel and collaborators apply a large incompleteness bias to their B-band TF application, largely based on the assumption that the TF intrinsic dispersion in B-band is as large as 0.7 mag. We have shown that the intrinsic TF dispersion is only  $\sim 0.30$  mag, even in B-band. In fact, there is no anti-correlation between the wavelength and the dispersion, as some papers had suggested earlier (e.g. Pierce & Tully 1988).

Third, some of the B-band TF distances to clusters have been measured with respect to the Virgo cluster whose distance modulus was assumed to be  $31.60 \pm 0.08$  mag (Tammann 1999). When there are nearly two dozen TF calibrators, there is no need to estimate TF distances based on one cluster distance.

Results from the KLUN (Kinematics of the Local Universe) survey have given  $H_0$  values around  $50\text{--}55 \text{ km s}^{-1} \text{ Mpc}^{-1}$  (cf. Theureau et al. 1997). This is a B-band, 21cm survey of  $\sim 2000$  spiral galaxies out to  $2000\text{--}3000 \text{ km s}^{-1}$ . The latest results from this survey (Ekholm et al. 1999) reported  $H_0 = 52 \pm 5 \text{ km s}^{-1} \text{ Mpc}^{-1}$  using the inverse diameter B-band TF relation, and  $53 \pm 6$  using the inverse magnitude B-band TF relation. The KLUN database includes field galaxies, which need to be corrected for Malmquist bias. They also found that their calibrator sample and the field sample followed different diameter slopes, and subsequently corrected for this effect. Both of these corrections decrease the value of  $H_0$ . Our TF analyses suggested that the cluster incompleteness bias was minimal, requiring a correction of only 2–3% in distance. Furthermore, we did not find a significant difference between the slopes of the calibrator and cluster samples.

We have also explored how systematic uncertainties can affect estimates of  $H_0$ . The main results are summarized as follows:

(1) Intrinsic dispersions of the TF relations are  $\sigma \simeq 0.19\text{--}0.25$  mag for  $BVRIH_{-0.5}$ . The dispersion does not seem to decrease significantly with wavelength as reported earlier.

(2) No color dependence of the TF relation was observed.

(3) The cluster population incompleteness bias was found to be small, typically  $\sim 0.05$  mag at most per cluster in distance modulus.

(4) The dependence of  $H_0$  on the TF slope is negligible.

(5) We found that our estimate of  $H_0$  is not sensitive to the choice of internal extinction correction. The estimates of  $H_0$  using three different extinction correction methods all agree well within  $1\sigma$  uncertainties.

(6) A very small dependence of the value of  $H_0$  on the metallicity dependence of the Cepheid PL relation was observed. When a metallicity dependence of  $\gamma = 0.24 \pm 0.16 \text{ mag dex}^{-1}$  is adopted,  $H_0$  decreases by 3%.

(7)  $H_0$  is not sensitive to the velocity field model adopted. We have used the CMB reference frame as a default case in measuring  $H_0$ . However, we have also examined the case in which the flow field was estimated using a three-attractor model. That yielded an  $H_0$  that is exactly the same as that obtained using the CMB velocities.

(8) The larger two databases, based on the I-band and H-band surveys, which are likely more statistically reliable than the other two, give Hubble constants that are different by 10%. We suggest that this difference arises from systematic photometric differences between the calibrators and cluster galaxies in  $H_{-0.5}$  magnitudes, which are circular aperture magnitudes. This clearly needs to be revisited in the future, possibly by obtaining deep H-band total magnitudes consistently for both the calibrators and cluster galaxies.

It is a pleasure to thank Martha Haynes for generously providing us with the 21cm line profiles. Also we would like to thank Riccardo Giovanelli, Brent Tully, Mike Pierce and Greg Bothun for discussions. We also thank Jeff Mader for assembling the initial database and references for our calibrator line-widths. S.S. acknowledges support from NASA through the Long Term Space Astrophysics Program, NAS-7-1260. L.M. acknowledges partial support by AURA through Gemini Fellowship No. GC-1003-95. L.F. acknowledges support by NASA through Hubble Fellowship grant HF-01081.01-96A awarded by the Space Telescope Science Institute, which is operated by the Association of Universities for Research in Astronomy, Inc., for NASA under contract NAS 5-26555. S.M.G.H. and P.B.S. acknowledge support from a NATO collaborative research grant (CRG960178). The work presented in this paper is based on observations with the NASA/ESA Hubble Space Telescope, obtained by the Space Telescope Science Institute, which is operated by AURA, Inc. under NASA contract No. 5-26555. Support for this work was provided by NASA through grant GO-2227-87A from STScI. This research has made use of the NASA/IPAC Extragalactic Database (NED) which is operated by the Jet Propulsion Laboratory, Caltech, under contract with the National Aeronautics and Space Administration.

## REFERENCES

- Aaronson, M., Mould, J.R., 1983, ApJ, 265, 1  
 Aaronson, M., Mould, J.R., Huchra, J.P., 1979, ApJ, 229, 1  
 Aaronson, M., Mould, J., Huchra, J., Sullivan, W.T., Schommer, R.A., Bothun, G.D., 1980, ApJ, 239, 12  
 Aaronson, M., Huchra, J.P., Mould, J.R., Tully, R.B., Fisher, J.R., Vanwoerden, H., Goss, W.M., Chamaraux, P., Mebold, U., Siegman, B., Berriman, G. and Persson, S.E., 1982, ApJS, 50, 241  
 Aaronson, M., Bothun, G., Mould, J.R., Huchra, J., Schommer, R.A., & Cornell, M.E., 1986, ApJ, 302, 536  
 Biviano, A., Giuricin, G., Mardirossian, F., Mezzetti, M., 1990, ApJS, 74, 325  
 Bernstein, G.M., Guhathakurta, P., Raychaudhury, S., Giovanelli, R., Haynes, M.P., Herter, T. & Vogt, N.P., 1994, AJ, 107, 1962  
 Bothun, G.D., Aaronson, M., Schommer, B., Mould, J., Huchra, J., Sullivan, W.T., 1985, ApJS, 57, 423  
 Bottinelli, L., Goughenheim, L., 1976, A&A, 51, 275

- Bottinelli, L., Goughenheim, L., Paturel, G., de Vaucouleurs, G., 1984, A&AS, 56, 381
- Bottinelli, L., Goughenheim, L., Paturel, G. & Teerikorpi, P., 1988, ApJ, 328, 4
- Braine, J. & Combes, F., 1992, A&A, 264, 433
- Bureau, M., Mould, J.R., & Staveley-Smith, L., 1996, ApJ, 463, 60
- Burstein, D., Willick, J.A., & Courteau, S., 1995, in “The Opacity in Spiral Disks”, ed. J.I. Davies and D. Burstein, Kluwer Academic Publishers
- Buta, R., 1988, ApJS, 66, 233
- Cardelli, J.A., Clayton, G.C. & Mathis, J.S., 1989, ApJ, 345, 245
- Corradi, R.L.M. & Capaccioli, M., 1991, A&AS, 90, 121
- Davis, L.E., & Seaquist, E.R., 1983, ApJS, 53, 269
- de Jong, R.S., 1997, PhD Thesis, Kapteyn Astronomical Institute
- de Vaucouleurs, G., de Vaucouleurs, A., & Corwin, J.R., 1976, Second Reference Catalog of Bright Galaxies (RC2)
- Dekel, A., 1994, ARA&A, 32, 371
- Dumke, M., Krause, M., Wielebinski, R., & Klein, U., 1995, A&A, 302, 691
- Ekholm, T., Teerikorpi, P., Theureau, G., Hanski, M., Paturel, G., Bottinelli, L., & Goughenheim, L., 1999, A&A, in press
- Eisenstein, D.J. & Loeb, A., 1996, ApJ, 459, 432
- Federspiel, M., Sandage, A. & Tammann, G.A., 1994, ApJ, 430, 29 (FST94)
- Federspiel, M., Tammann, G.A., & Sandage, A., 1998, ApJ, 495, 115
- Ferrarese, L. et al., 1998, ApJ, 507, 655
- Ferrarese, L. et al., 2000a, submitted
- Ferrarese, L. et al., 2000b, submitted
- Fouque, P., Bottinelli, L., Goughenheim, L., Paturel, G., 1990, ApJ, 349, 1
- Freedman, W.L., 1990, ApJ, 355, L35
- Freedman, W.L. et al. 1994, ApJ, 427, 628
- Freedman, W.L. et al. 2000, ApJ, in preparation
- Fukugita, M., Okamura, S., Tarusawa, K., Rood, H.J., Williams, B.A., 1991, ApJ, 376, 8
- García-Gómez & Athanoussla, 1991, A&AS, 89, 159
- Gibson, B.G. et al. 1999, ApJ, in press
- Gibson, B.G. et al. 2000, submitted
- Giovanelli, R., 1997, in “The Extragalactic Distance Scale”, M.Livio, M.Donahue, and N.Panagia, eds., Cambridge University Press
- Giovanelli, R., & Haynes, M.P., 1985, AJ, 90, 2445
- Giovanelli, R., Haynes, M.P., Salzer, J.J., Wegner, G., Da Costa, L.N., Freudling, W., 1994, AJ, 107, 2036
- Giovanelli, R., Haynes, M.P., Herter, T., Vogt, N.P., Wegner, G., Salzer, J.J., Da Costa, L.N., Freudling, W., 1997a, AJ, 113, 22
- Giovanelli, R., Haynes, M.P., Herter, T., Vogt, N.P., Da Costa, L.N., Freudling, W., Salzer, J.J., Wegner, G., 1997b, AJ, 113, 53
- Giovanelli, R., Haynes, M.P., Salzer, J.J., Wegner, G., DaCosta, L.N., Freudling, W., 1998, AJ, 116, 2632
- Giraud, E., 1986, A&A, 164, 17
- Gould, A., 1993, ApJ, 412, L55
- Gould, A., 1994, ApJ, 426, 542
- Graham, J.A. et al., 1997, ApJ, 477, 535
- Graham, J.A. et al., 1999, ApJ, 516, 626
- Guhathakurta, P., van Gorkom, J.H., Kotanyi, C.G., & Balkowski, C., 1988, AJ, 96, 851
- Han, M., 1991, PhD Thesis, California Institute of Technology
- Han, M., 1992, ApJ, 391, 617
- Han, M. & Mould, J.R., 1992, ApJ, 396, 453
- Holmberg, E. 1958, Medd Lund Obs II, No. 136
- Huchtmeier, W.K. & Richter, O.G., 1988, A&A, 203, 237
- Hughes, S.M.G. et al., 1998, ApJ, 501, 32
- Jackson, J.M., Snell, R.L., Ho, P.T.P., & Barrett, A.H., 1989, ApJ, 337, 680
- Jorsater, S. & van Moorsel, G., 1995, AJ, 110, 2037
- Kelson, D.D. et al., 1999, ApJ, 514, 614
- Kelson, D.D. et al., 2000, ApJ, submitted
- Kennicutt, R.C., 1999, ARA&A, 36
- Kennicutt, R.C. et al., 1998, ApJ, 498, 181
- Kent, S.M., 1983, ApJ, 266, 562
- Kraan–Korteweg, R.G., Cameron, L.M., and Tammann, G.A., 1988, ApJ, 331, 620
- Krumm, N., & Salpeter, E.E., 1979, AJ, 84, 1138
- Landy, S.D., & Szalay, A.S. 1992, ApJ, 391, 494
- Lauer, T.R. & Postman, M., 1994, ApJ, 425, 418
- Lynden-Bell, D., Burstein, D., Davies, R.L., Dressler, A., Terlevich, R.J., & Wegner, G., 1988, ApJ, 326, 19
- Macri, L.M. et al., 1999, ApJ, 521, 155
- Macri, L.M. et al., 2000, ApJ, in preparation
- Madore, B.F. & Freedman, W.L., 1991, PASP, 103, 933
- Madore, B.F. et al., 1999, ApJ, 515, 29
- Mathewson, D.S. & Ford, V.L., 1996, ApJS, 107, 97
- Moore, E.M. & Gottesman, S.T., 1998, MNRAS, 294, 353
- Mould, J.R., Aaronson, M., Huchra, J.P., 1980, ApJ, 238, 458
- Mould, J.R., Han, M & Bothun, G., 1989, ApJ, 347, 112
- Mould, J.R., Sakai, S., Hughes, S. & Han, M., 1996, Space Telescope Institute Symposium Series, Vol. 10, p. 158. ed. Livio, Donahue, and Panagia
- Mould, J.R. et al., 1998, ApJ, in press
- Mould, J.R. et al., 2000, ApJ, submitted
- Öpik, E., 1922, ApJ, 55, 406
- Peletier, R.F., & Willner, S.P., 1993, ApJ, 418, 626
- Phelps, R.L. et al., 1998, ApJ, 500, 763
- Pierce, M.J., & Tully, B.R., 1988, ApJ, 330, 579
- Pierce, M.J. & Tully, B.R., 1992, ApJ, 387, 47
- Rawson, D.M. et al. 1997, ApJ, 490, 517
- Reif, K., Mebold, U., Goss, W.M., van Woerden, H., & Siegmán, B., 1982, A&AS, 50, 451
- Riess, A.G., Press, W.H., & Kirshner, R.P., 1995, ApJ, 445, 91
- Roberts, M.S., 1969, AJ, 74, 859
- Roberts, M.S., 1978, in Vol. IX, *Stars and Stellar Systems*, ed. by A. Sandage, M.Sandage, & J. Kristian, Chicago: U. of Chicago Press, P.309
- Rood, H.J., & Williams, B.A., 1993, MNRAS, 263, 211
- Saha, A., Sandage, A., Labhardt, L., Tammann, G.A., Macchetto, F.D. and Panagia, N., 1996, ApJ, 466, 55
- Saha, A., Sandage, A., Tammann, G.A., Labhardt, L., Macchetto, F.D. & Panagia, N., 1999, ApJ, in press
- Sakai, S. et al. 1999, ApJ, in press
- Sandage, A., 1994, ApJ, 430, 13
- Sandage, A., Tammann, G.A., 1976, ApJ, 210, 7
- Sandage, A., Tammann, G.A., 1984, Nature, 307, 326
- Schechter, P.L., 1980, AJ, 85, 801
- Schlegel, D.J., Finkbeiner, D.P., & Davis, M. 1998, ApJ, 500, 525
- Schöniger, F. & Sofue, Y., 1994, A&A, 283, 21
- Silbermann, N.A. et al. 1996, ApJ, 470, 1
- Silbermann, N.A. et al. 1999, ApJ, 515, 1
- Silk, J., 1996, in “the Universe at High z, Large Scale Structure and the Cosmic Microwave Background”, E.Martínez-González, & J.-L. Sanz, eds., Springer-Verlag, in press
- Shanks, T., 1997, MNRAS, 290, 77
- Strauss, M.A., & Willick, J.A., 1995, Physics Reports, 261, 271
- Tammann, G.A., 1999, IAU Symposium #183, “Cosmological Parameters and the Expansion of the Universe”
- Tanvir, N.R., Shanks, T., Ferguson, C and Robinson, R.T., 1995, Nature, 377, 27
- Teerikorpi, P., 1984, A&A, 141, 407
- Teerikorpi, P., 1987, A&A, 173, 39
- Teerikorpi, P., 1997, ARA&A, 35, 101
- Theureau, G., 1998, A&A, 331, 1
- Theureau, G., Hanski, M., Ekholm, T., Bottinelli, L., Goughenheim, L., Paturel, G., Teerikorpi, P., 1997, A&A, 322, 730
- Tormen, G., Burstein, D., 1995, ApJS, 96, 123
- Tully, B.R., 1999, IAU Symposium #183
- Tully, R.B. & Fisher, J.R., 1977, A&A, 54, 661
- Tully, R.B. & Fouque, P., 1985, ApJS, 58, 67
- Tully, R.B., Mould, J.R., Aaronson, M., 1982, ApJ, 257, 527
- Tully, R.B., Pierce, M.J., Huang, J., Saunders, W., Verheijen, M.W., Witchalls, P.L., 1998, AJ, 115, 2264 (T98)
- Turner, A. et al., 1998, ApJ, 505, 207
- Valentijn, E.A., 1990, Nature, 346, 153
- Visvanathan, N., 1982, Proc. ASA, 4, 419
- Visvanathan, N., 1983, ApJ, 275, 430
- Walsh, W. 1999, private communications
- Wevers, B.M.H.R., Appleton, P.N., Davies, R.D., & Hart, L., 1984, A&A, 140, 125
- Willick, J.A., 1991, PhD Thesis, University of California, Berkeley
- Willick J.A., Courteau, S., Faber, S.M., Burstein, D., Dekel, A., & Kolatt, T., 1996, ApJ, 457, 460
- Yahil, A., Tammann, G.A. & Sandage, A., 1977, ApJ, 217, 903
- Yasuda, N., Fukugita, M., Okamura, S., 1997, ApJS, 108, 417

## APPENDIX

## A. INTERNAL EXTINCTION CORRECTIONS

We briefly review three different methods for correcting for internal extinction. The “internal extinction” correction here strictly refers to the relative correction of spiral galaxy magnitudes to the face-on orientation; we do not apply an absolute, total extinction correction to any of our galaxies.

The first such correction to consider is that of Han (1992). Using a sample of 284 spiral galaxies in I-band, he presented a set of parametric expressions as follows:

$$A_{int,I}^{Han} = \begin{cases} -0.73 \log(b/a) & T \leq 3 \\ -0.90 \log(b/a) & T = 4, 5 \\ -0.51 \log(b/a) & T > 6 \end{cases} \quad (A1)$$

where  $(b/a)$  is the minor-to-major axis ratio, expressed by  $(1-e)$ .

G97 examined again several hundred Sbc-Sc galaxies and derived a more complicated set of parametric formulae for internal extinction corrections which depended on both the inclination and the size of the galaxies. The basic idea behind their correction is that the light traverses a longer path in a larger galaxy, increasing the internal extinction; the larger the galaxy is, the more correction is needed. The internal extinction expression given by G97 is:

$$A_{int,I}^{G97} = \gamma(\log W) \log(a/b) \quad (A2)$$

where  $\gamma$  is parametrized as a function of linewidth, whose values are given in Table 3 of G97 and vary between 0.57 and 1.70. In addition to the size-dependent correction, G97 suggests a constant offset for galaxies of earlier types.

$$\beta = \begin{cases} 0.10 & T = 1, 2 \\ 0.32 & T = 3 \\ 0.0 & \text{otherwise.} \end{cases} \quad (A3)$$

The total extinction is thus given by  $A_{int}^{G97} + \beta$ .

## B. INCLINATIONS

In Table B1, we summarize the inclination information compiled from previously published data for each galaxy. The columns include: (1) name of the galaxy; (2) photometric inclination angles published with references indicated by numbers in brackets; and (3) kinematical inclination angles.

## C. QUADRATIC TULLY-FISHER RELATIONS

Several papers have investigated the possibility of a Tully-Fisher relation being a quadratic relation (cf: Mould, Han and Bothun 1989). Pierce and Tully (1988) noted that the TF relation at faint end tends to curve downward. Giovanelli et al. (1997) however noted that their sample of several hundred galaxies showed no such trend. We have fitted a quadratic equation to each  $BVRIH$  Tully-Fisher correlation and obtained the following results where  $w = \log W_{20\%}^C - 2.5$ :

21 -19.8380 -7.94259 8.11011 17 -20.4028 -8.41765 6.44754 21 -20.6891 -9.34836 9.29448 21 -21.1989 -10.19832 11.5500 20 -21.8610 -12.1775 12.7621

$$B_T^C = -19.84 - 7.94w + 8.11w^2 \quad (C1)$$

$$V_T^C = -20.40 - 8.42w + 6.45w^2 \quad (C2)$$

$$R_T^C = -20.69 - 9.35w + 9.29w^2 \quad (C3)$$

$$I_T^C = -21.20 - 10.20w + 11.55w^2 \quad (C4)$$

$$H_{-0.5}^C = -21.86 - 12.18w + 12.76w^2 \quad (C5)$$

In Figure 13, these fits are shown by solid lines. In comparison, linear fits (Equations 6–10) are drawn by dashed lines.

If one were to use the quadratic equation instead, distances to individual galaxies may change slightly, especially for those with large linewidth ( $\log W > 2.6$ ) or smaller linewidths ( $\log W < 2.3$ ). However, its effect on the value of  $H_0$  should be negligible for two reasons: (1) the distance to the cluster should not change in the mean, and (2) we are restricting the cluster sample galaxies to those in the range of  $2.3 \leq \log W \leq 2.6$ . Because the number statistics are not sufficient to conclude whether the TF relation is quadratic or not, and also because the calibrator sample spans a rather small range of linewidths, we will not use above equations (C1) through (C5) in our further analysis.

TABLE B 1  
Inclination Angles

NGC	Photometric <sup>a</sup> (Degrees)	Kinematical <sup>a</sup> (Degrees)
NGC 224	72 (1,5), 78 (2,3,4)	75–78 (18)
NGC 598	51 (1), 55 (3), 54 (2)	55 (6)
NGC 925	55 (7), 52 (8,9), 51 (10), 54 (11), 57 (2)	55 (12)
NGC 1365	57 (1,13), 61 (14), 63 (11), 44 (15)	40 (16)
NGC 1425	62 (1), 66 (15), 64 (17)	
NGC 2090	59 (1), 60 (13), 62 (17)	
NGC 2403	53 (1), 55 (3), 60 (4), 61 (2)	60 (12), 50 (6)
NGC 2541	58 (1)	
NGC 3031	59 (1,9)	58 (6)
NGC 3198	65 (1,5,3)	70 (12)
NGC 3319	56 (1,19)	59 (26)
NGC 3351	47 (1,20)	34 (6), 40 (21)
NGC 3368	45 (1)	
NGC 3621	50 (1,13), 62 (3), 65 (11)	65 (22)
NGC 3627	62 (1)	65 (6)
NGC 4414	54 (1)	50–70 (23)
NGC 4535	43 (1), 45 (5)	40 (24)
NGC 4536	64 (5), 65 (7), 69 (20)	
NGC 4548	36 (1)	42 (24)
NGC 4725	45 (1)	53 (12)
NGC 7331	70 (1,5), 71 (7,23)	75 (6)

<sup>a</sup> (1) Bottinelli et al. 1984, (2) Shanks et al. 1997, (3) Huchtmeier & Richter 1988, (4) Rood & Williams 1993, (5) Biviano et al. 1990, (6) Garcia–Gomez & Athanoussla 1991, (7) Krumm & Salpeter 1979, (8) Davis et al. 1983, (9) Giraud 1986, (10) Giovanelli & Haynes 1985, (11) Tully 1988, (12) Wevers et al. 1984, (13) Reif et al. 1982, (14) Schoniger & Sofue, 1994, (15) Bureau et al. 1996, (16) Jorsater & van Moorsel 1995, (17) Mathewson et al. 1996, (18) Corradi & Capaccioli 1991, (19) Davis & Seaquist 1983, (20) Jackson et al. 1989, (21) Buta 1988, (22) Walsh 1999, (23) Braine & Combes 1993, (24) Guhathakurta et al. 1988, (25) Dumke et al. 1995. (26) Moore & Gottesman, 1998

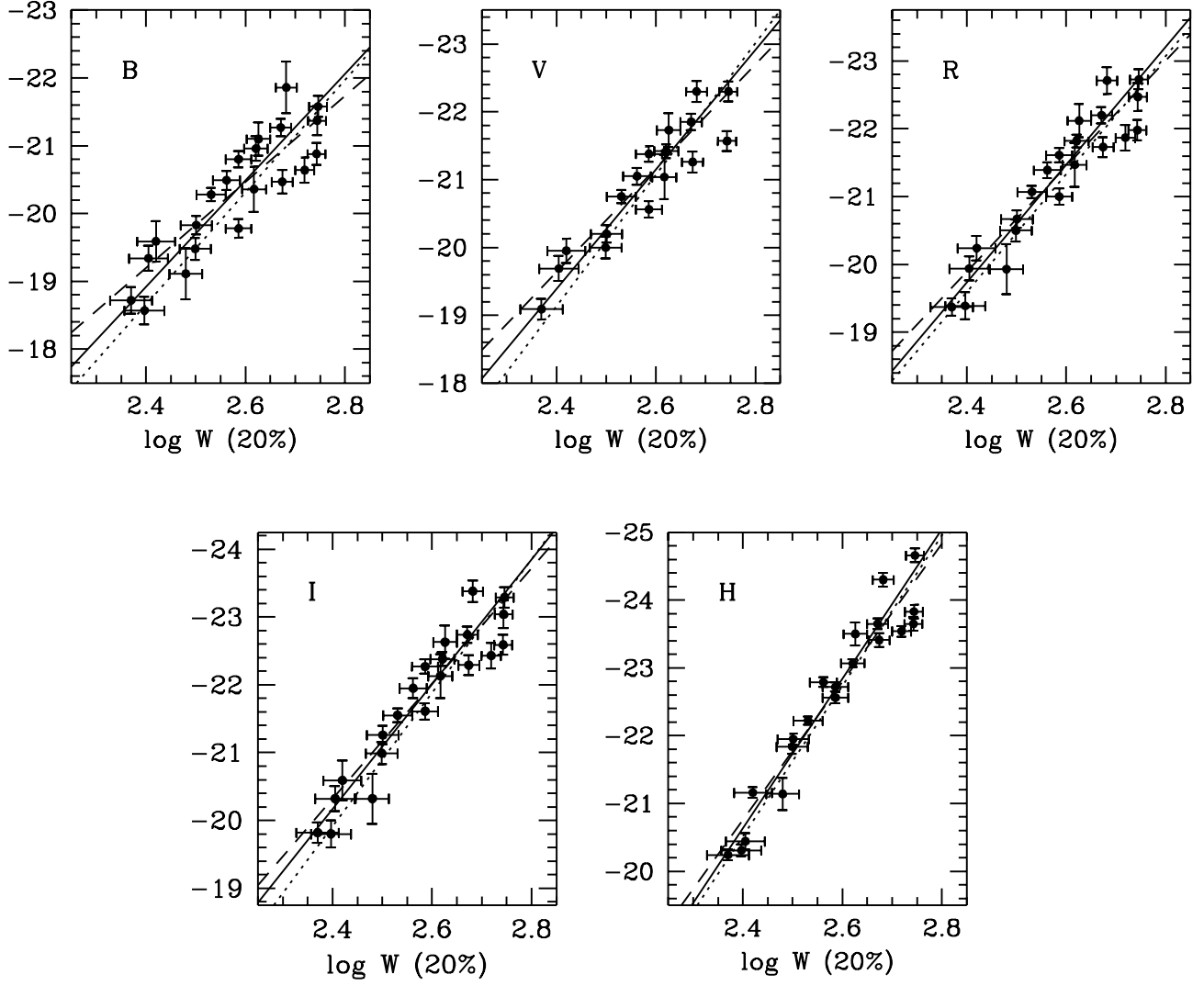


FIG. 1.— BVRIH<sub>0.5</sub> Tully-Fisher Relations for spiral galaxies with Cepheid distances, using 20% linewidth. Solid lines represent the bivariate fits, while the dotted and dashed lines represent inverse and direct fits.

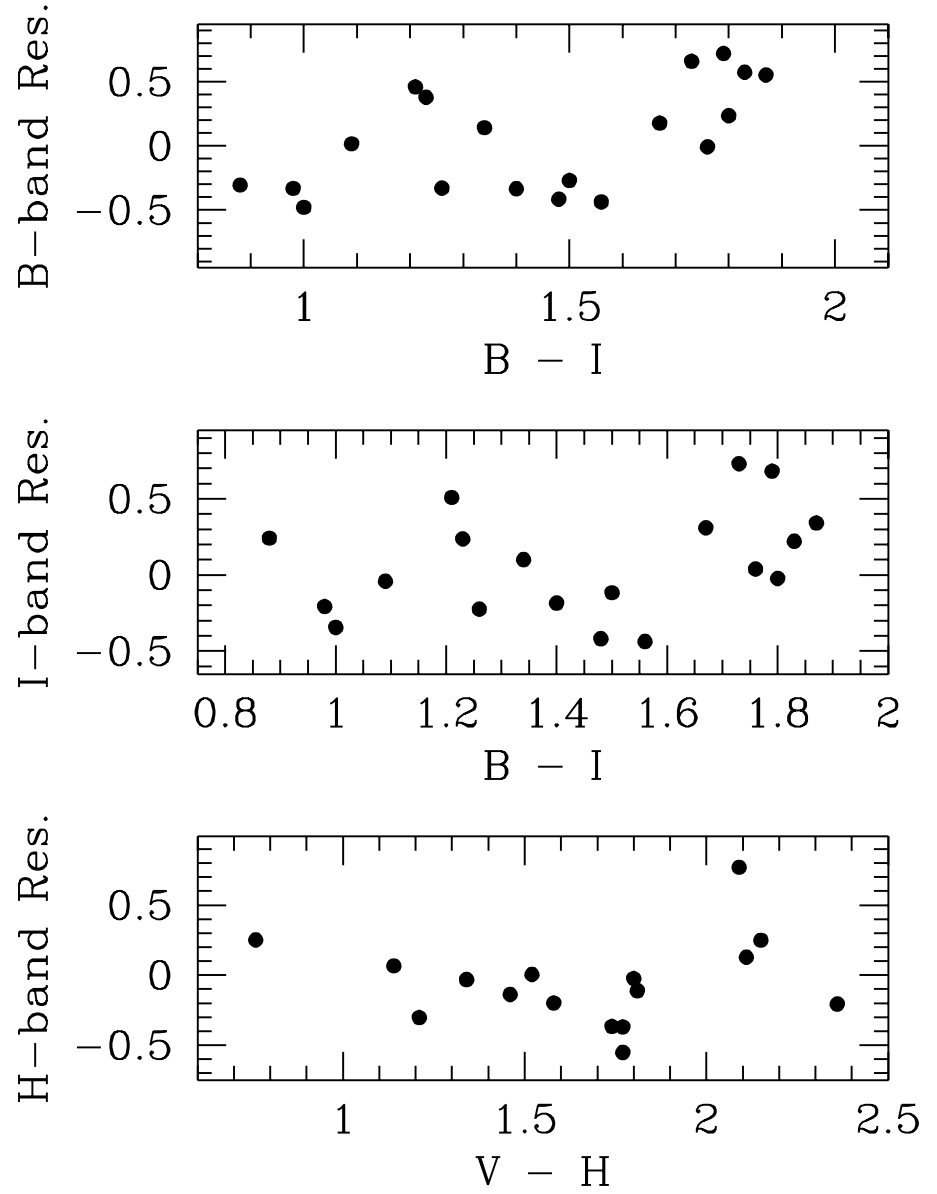


FIG. 2.— Observed minus predicted absolute magnitude as a function of color. Although the sample is small, there is no obvious dependence of the TF relation on color.

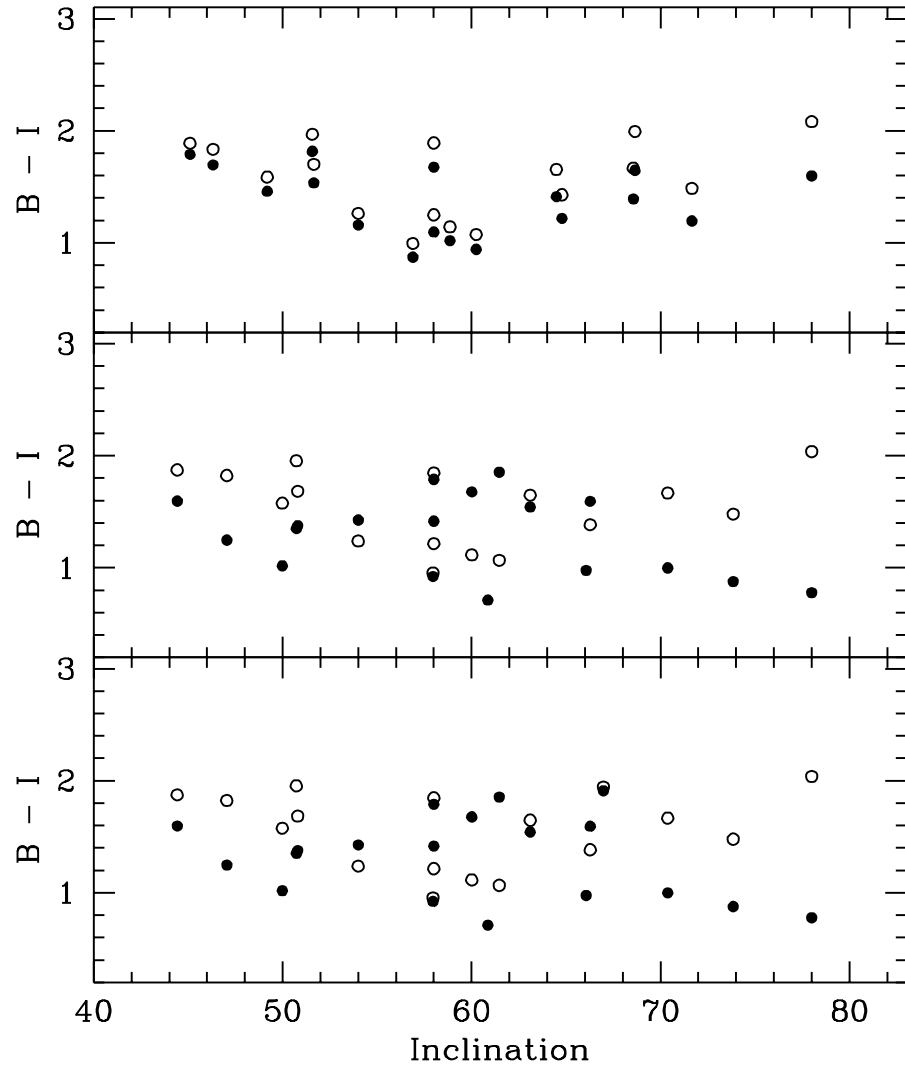


FIG. 3.— Color dependence on inclination for TF calibrator galaxies. Solid circles represent the correlations after correcting for the internal extinction using Tully et al.’s method (top), Han’s method (middle) and Giovanelli et al.’s method (bottom). Open circles are for the colors uncorrected for internal extinction. If the internal extinction correction were “correct”, this correlation should have zero slope.

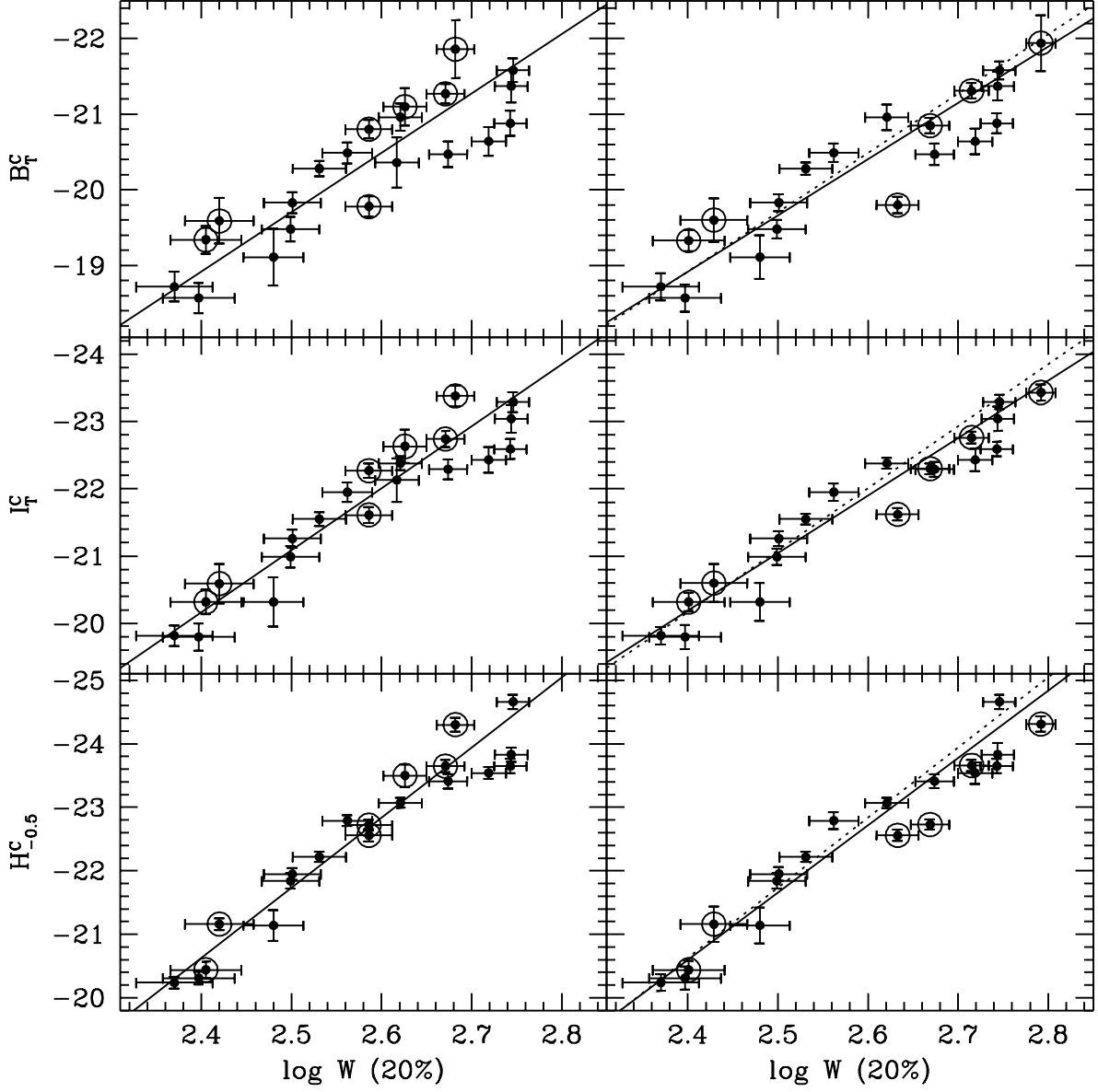


FIG. 4.— (*left*): B, I and H-band Tully–Fisher relations in which the photometric inclination angles were used. The barred galaxies are indicated by open circles. The solid lines represent the TF fit through all the galaxies, while the dashed lines the fit using only the barred galaxies. (*right*): B, I and H-band TF relations in which the kinematical inclination angles were adopted for barred galaxies only. Their TF fits are shown by solid lines. The dotted lines are the fits to all the galaxies using the photometric inclination angles (solid lines on the left plots). The zero point change in, for example, the I-band TF relation is 0.01 mag.



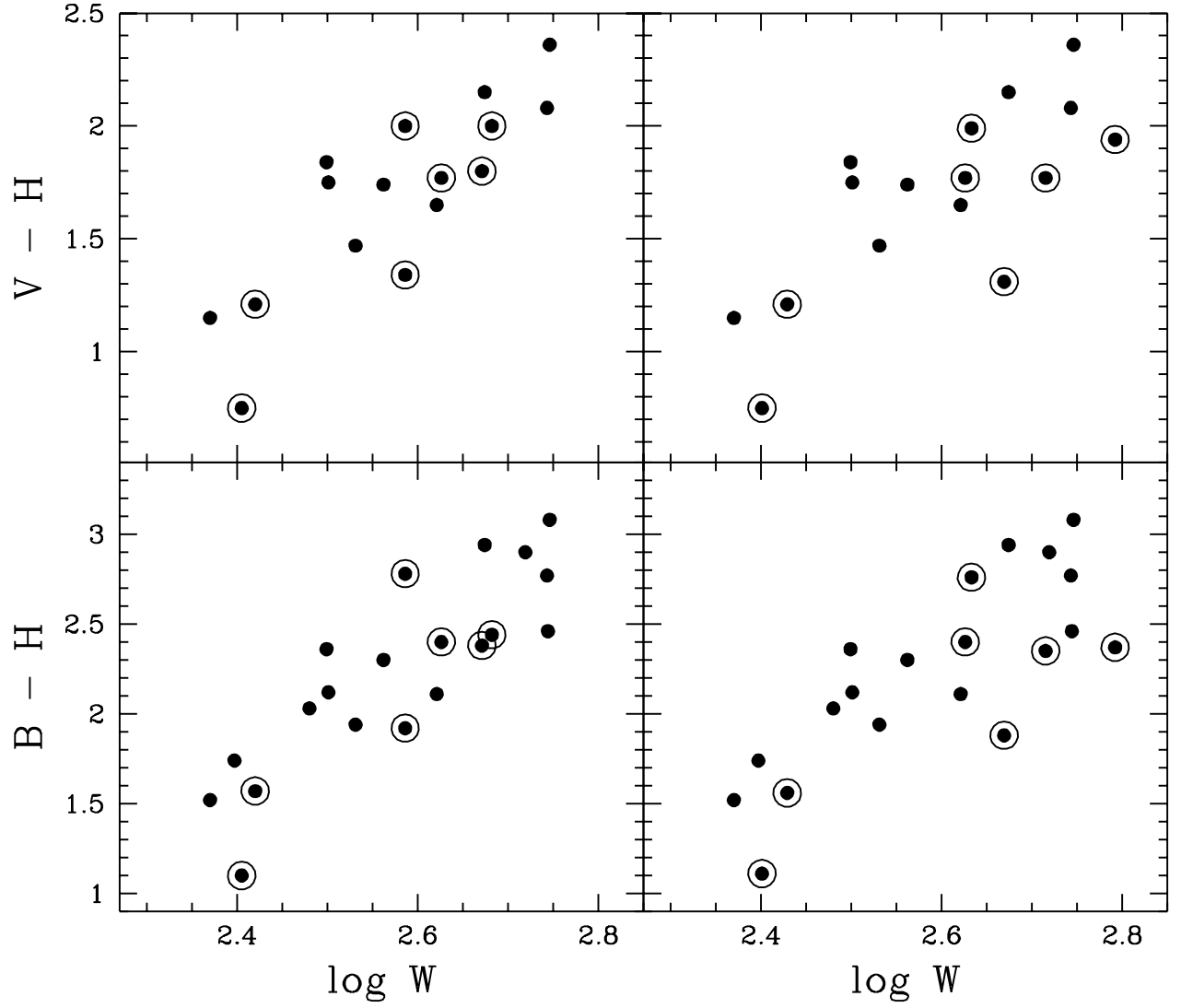


FIG. 5.— The  $V-H$  and  $B-H$  color distributions of the local calibrators. The barred galaxies are indicated by open circles. On the left, the magnitudes were corrected using the photometric inclination angles, while for those shown on the right side, the kinematical inclination angles were substituted for the barred galaxies.

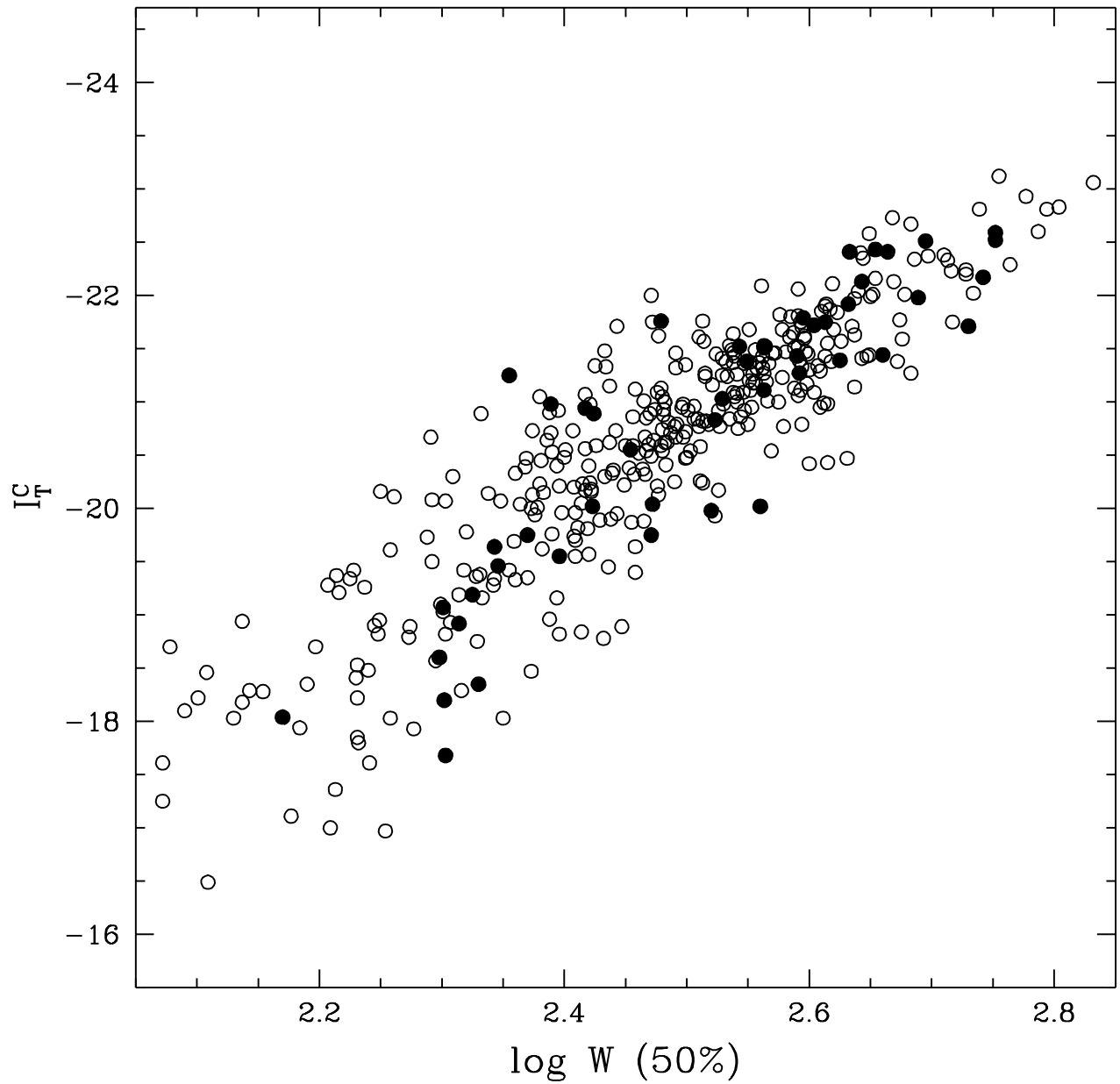


FIG. 6.— I-band Tully–Fisher relation for the cluster survey galaxies. The solid circles represent those galaxies classified as barred.

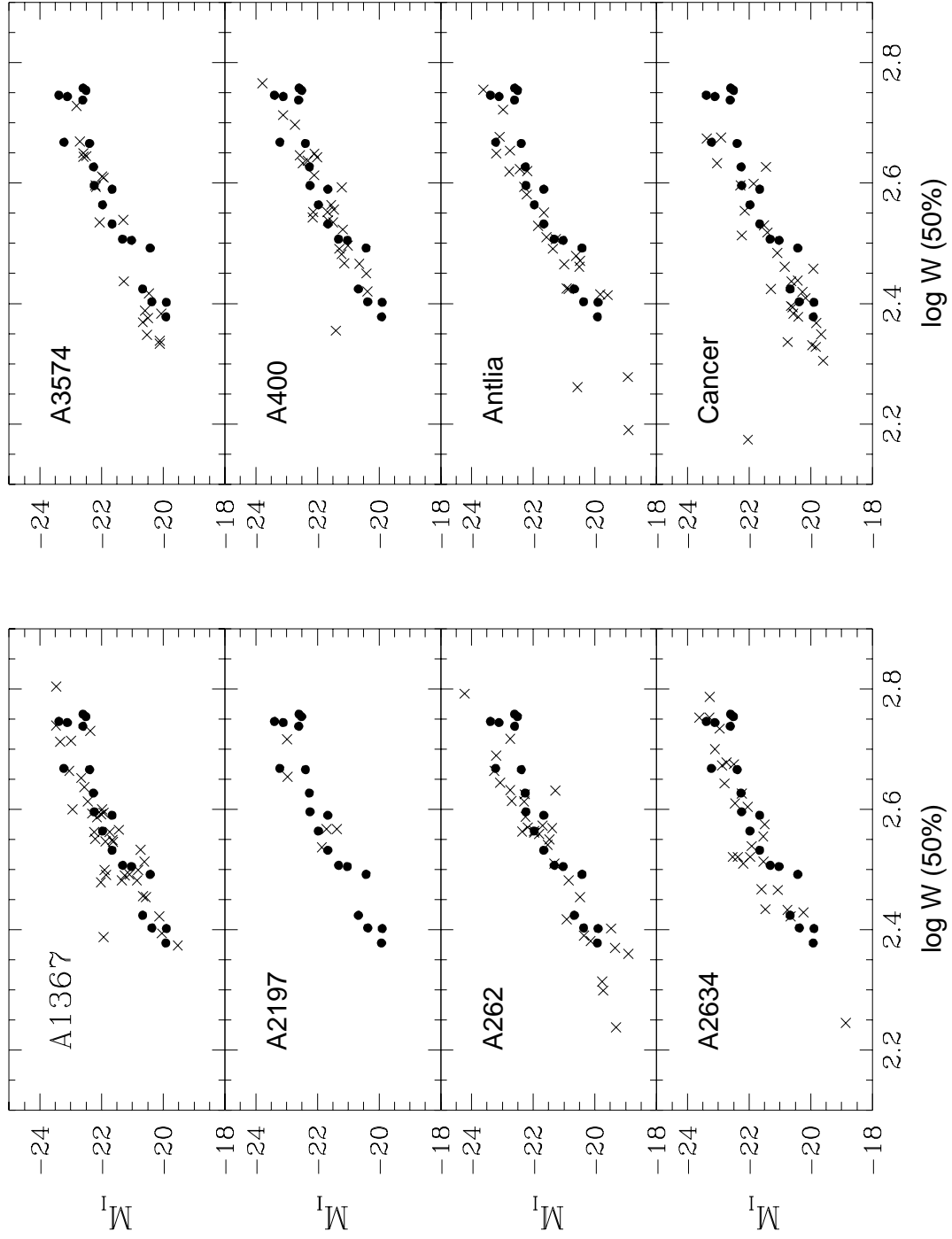


FIG. 7.— Examples of comparisons of the calibration galaxies (solid circles) with the cluster galaxies in the I-band survey (crosses).

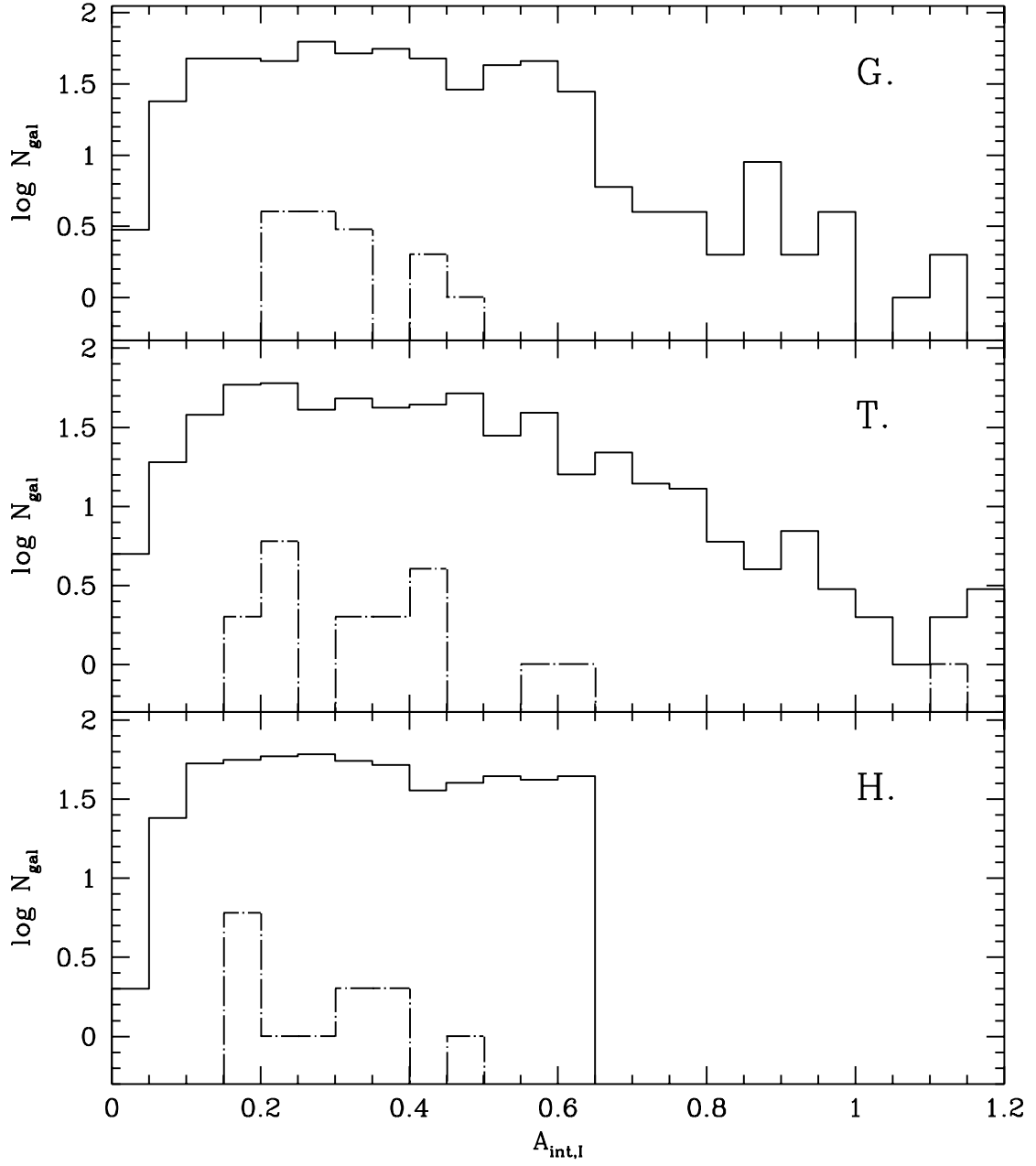


FIG. 8.— Comparison of distributions of internal extinction corrections: using Giovanelli et al (top), Tully et al. (middle) and Han’s method (bottom). The solid histograms represent the distributions for cluster galaxies, while the dotted–dashed histograms are for the calibrators. In our analysis, we exclude any galaxies whose internal extinction exceeds 0.6 mag.

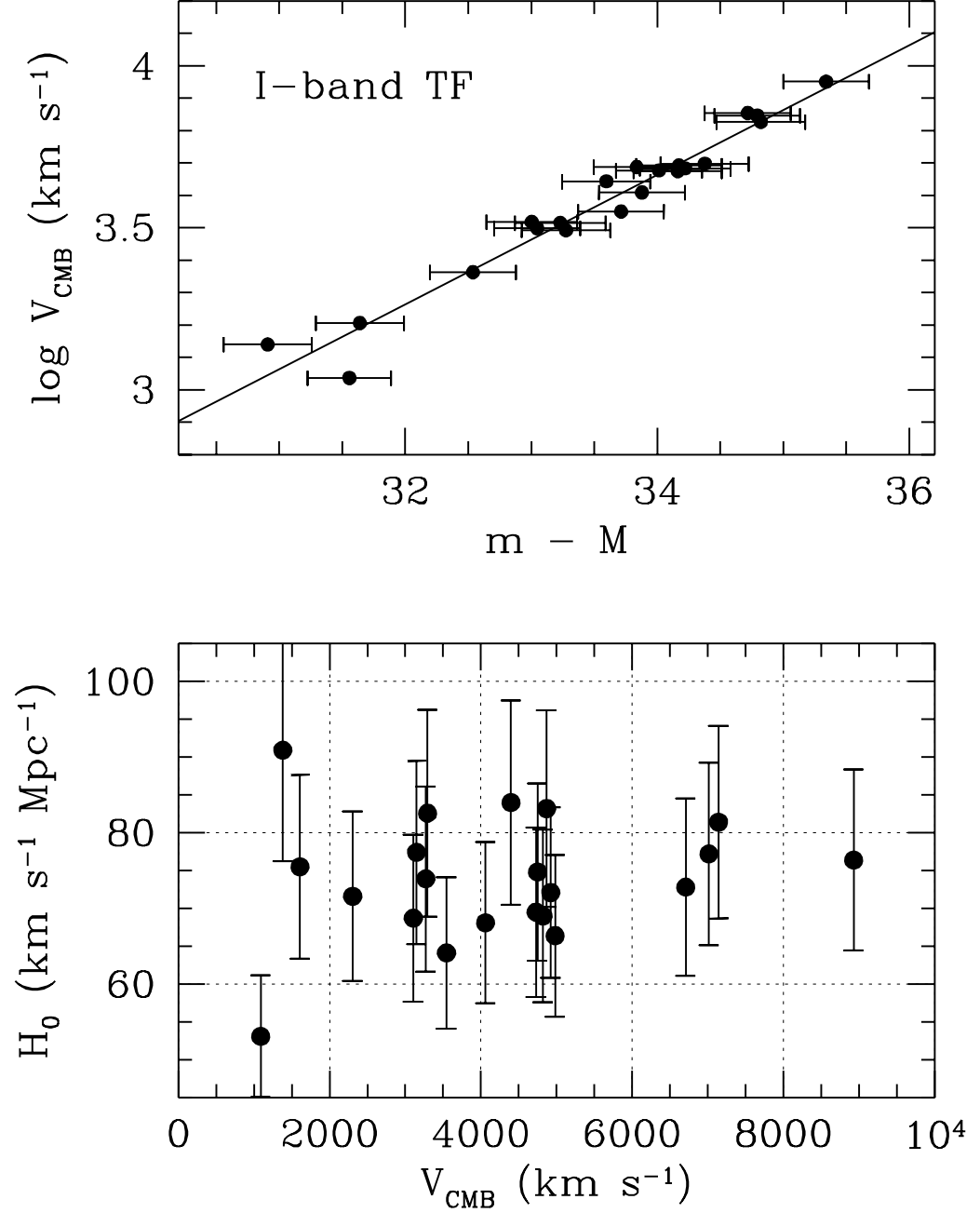


FIG. 9.— A  $\log D$ – $\log V$  relation for I-band clusters (top). A straight line represents  $H_0 = 73 \text{ km s}^{-1} \text{ Mpc}^{-1}$ . The bottom figure shows  $H_0$  as a function of velocity in the CMB reference frame. Taking the mean of clusters with  $V_{\text{cmb}} \geq 2000 \text{ km s}^{-1}$ , we obtain  $H_0 = 73 \pm 2 \text{ (random) km s}^{-1} \text{ Mpc}^{-1}$ .

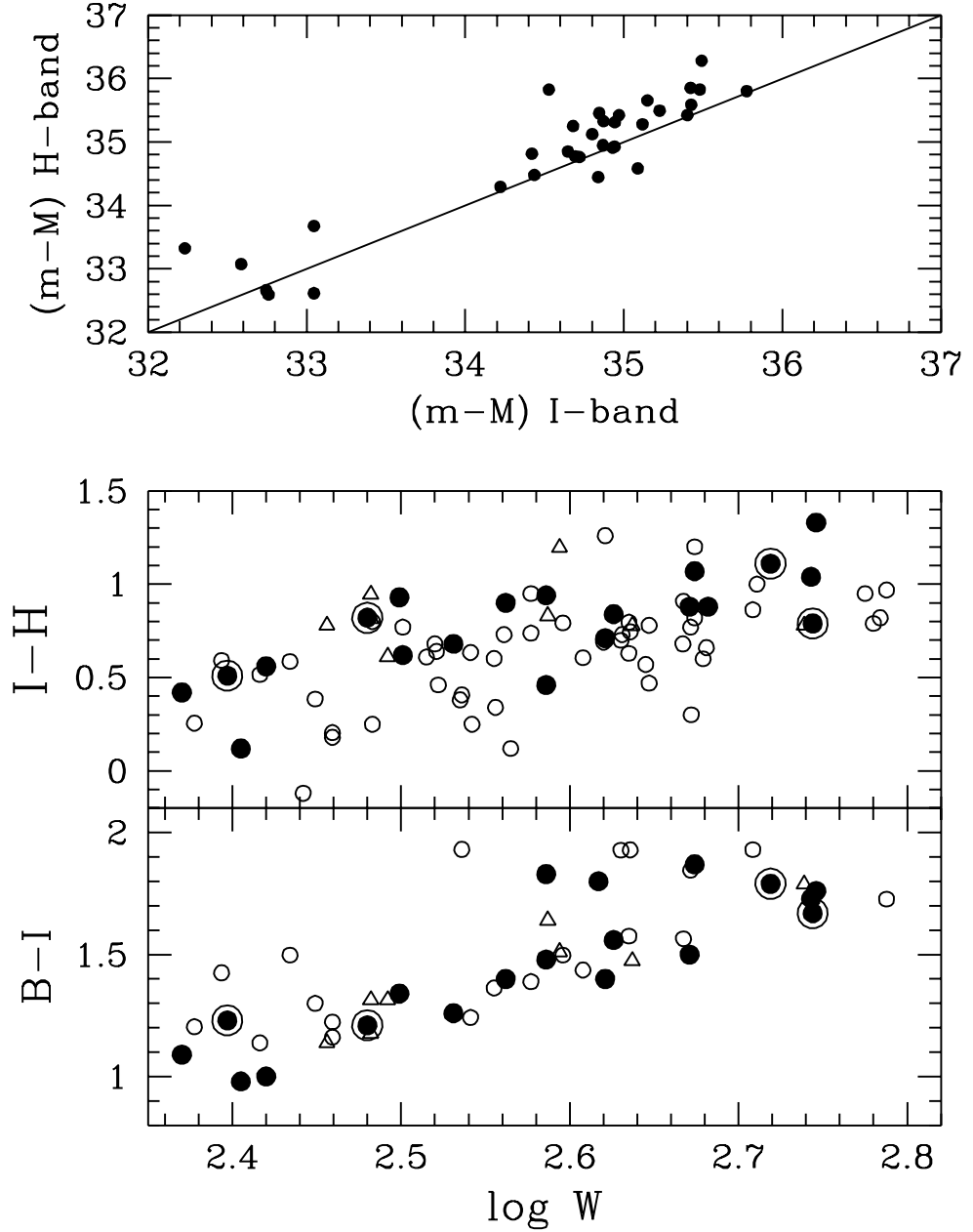


FIG. 10.— *Top:* Comparison of distance moduli derived from the I-band and H-band TF relations for galaxies that are included in both surveys. The solid line represents an one-to-one correspondence and is not a fit through the data. *Middle:* The  $I-H_{0.5}$  color distribution as a function of logarithmic linewidth for Virgo and Ursa Major galaxies (open squares) from Pierce & Tully (1988), and A1367, A400 and Coma galaxies whose photometric data (open triangles) were compiled from the G97 and B85 databases. The local calibrators are overplotted with solid circles. Note that the local calibrators are located on the red edge of the correlation for the cluster galaxies. *Bottom:*  $B-I$  color as a function of linewidth for the same set of galaxies as in the middle figure. The local calibrators are overplotted (solid circles). Four galaxies used by PT88 whose Cepheid distances were measured from ground are indicated by solid circles overplotted with open circles.

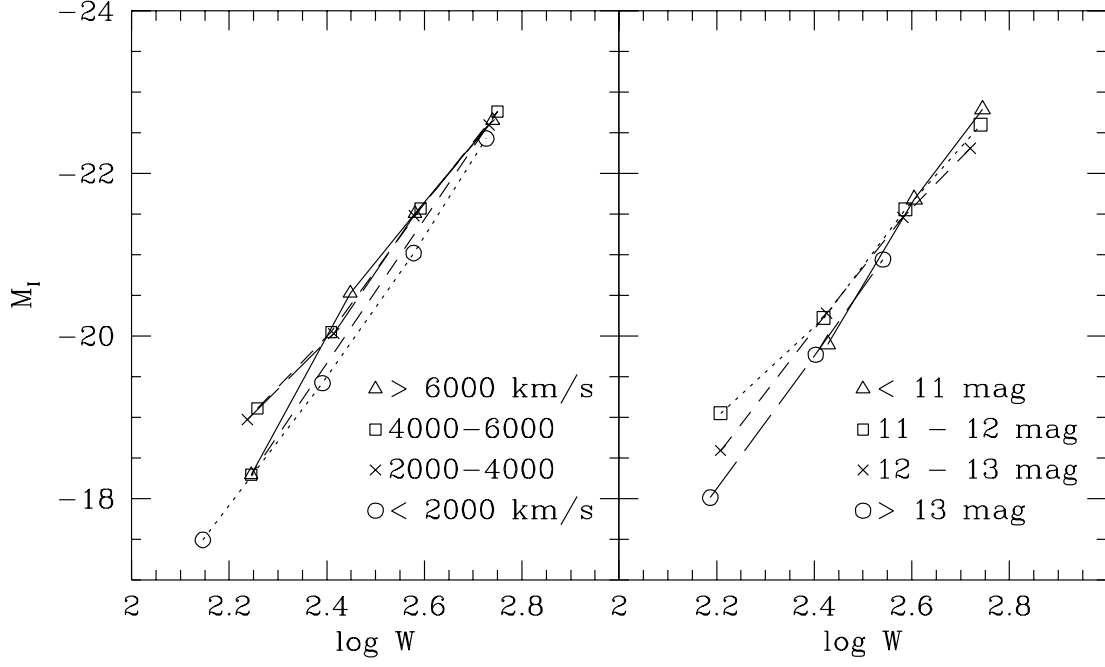


FIG. 11.— I-band Tully-Fisher relations for samples grouped by velocities in the CMB reference frame (left), and grouped by apparent magnitudes (right). The absolute magnitudes were calculated assuming  $H_0 = 100 \text{ km sec}^{-1} \text{ Mpc}^{-1}$  and that velocities give distances to first order. With an exception of the nearest sample, there seems to be no dependence of Tully-Fisher zero point on the sample. For the nearest sample ( $< 2000 \text{ km s}^{-1}$ ), the offset is likely due to the fact that its velocity field is not characterized well by the CMB model.

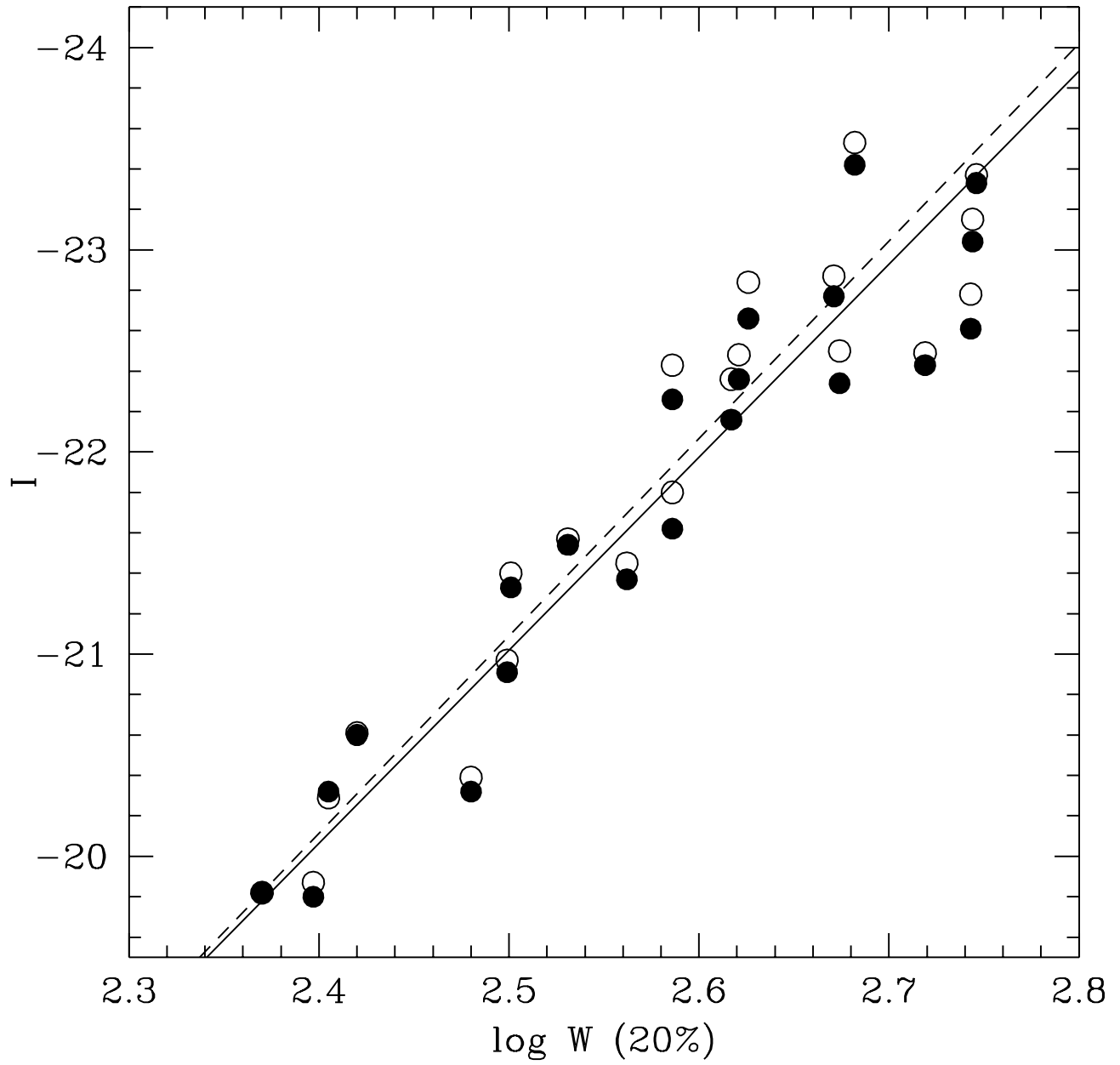


FIG. 12.— I-band- $\log W_{20}$  Tully–Fisher relation (solid circles). Open circles present the luminosity–linewidth relation for same galaxies, except that their distances have been adjusted to incorporate the metallicity dependence of the Cepheid PL relation, using  $\gamma = 0.24 \text{ mag dex}^{-1}$  (see text).



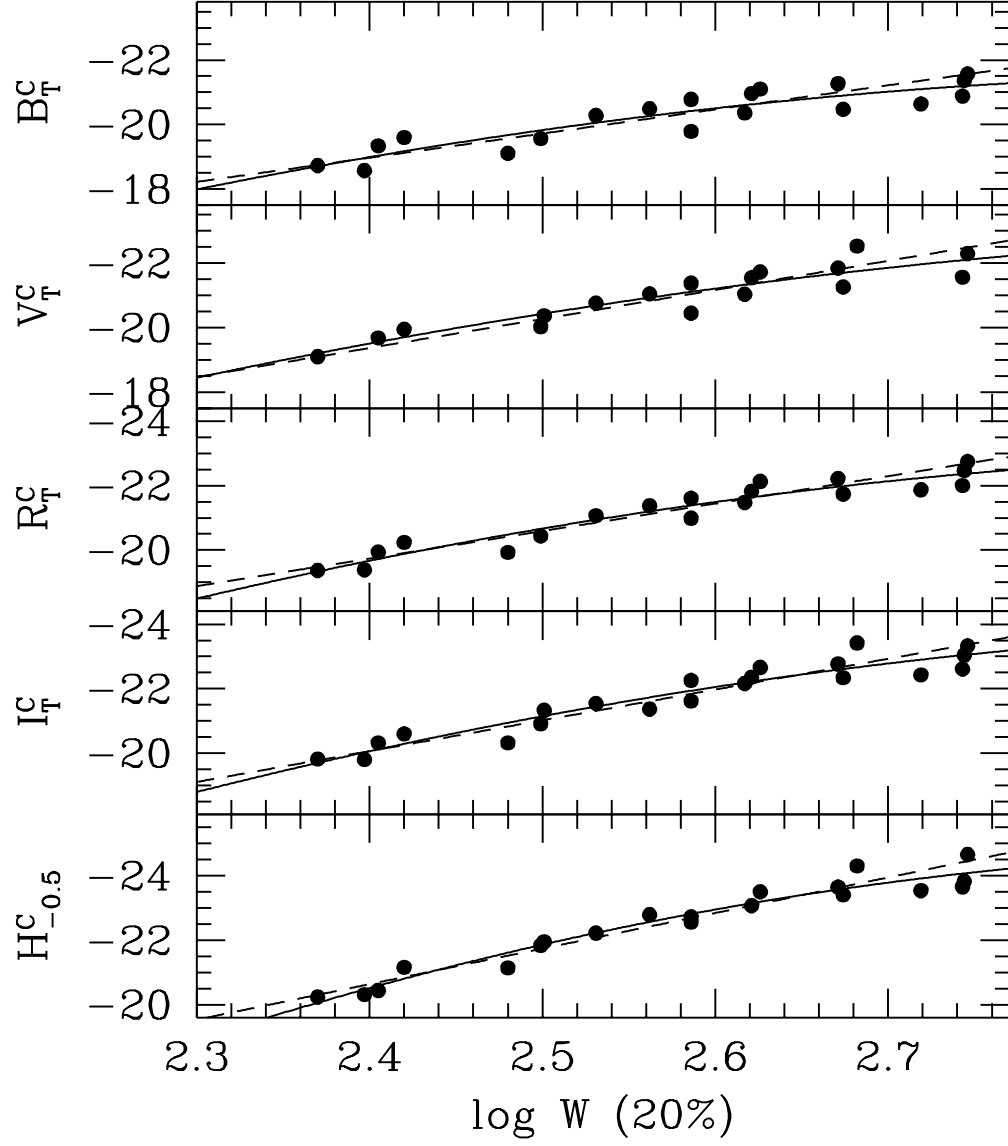


FIG. 13.— The solid line in each Tully–Fisher relation represents a quadratic fit while the dashed line is the linear relation (Equations 6 – 10). Applying the I-band quadratic TF relation to the cluster data, we obtain  $H_0 = 75 \pm 5 \text{ km s}^{-1} \text{ Mpc}^{-1}$ .